Geochemistry Geophysics Geosystems G3
AN ELECTRONIC JOURNAL OF THE EARTH SCIENCES
Published by AGU and the Geochemical Society

Article
Volume 6, Number 6
24 June 2005
Q06009, doi:10.1029/2004GC000896
ISSN: 1525-2027

Submarine fault scarps in the Sea of Marmara pull-apart (North Anatolian Fault): Implications for seismic hazard in Istanbul

Rolando Armijo, Nicolas Pondard, Bertrand Meyer, and Gulsen Uçarkus
Laboratoire de Tectonique, UMR 7578, CNRS, IPGP, 4 Place Jussieu, F-75252 Paris Cedex 05, France (armijo@ipgp.jussieu.fr)

Bernard Mercier de Lépinay
Geosciences-Azur, UMR 6526, CNRS Université Nice Sophia-Antipolis, Valbonne, France

Jacques Malavieille and Stéphane Dominguez
Laboratoire de Dynamique de la Lithosphère, UMR 5573, CNRS, Université Montpellier 2, Montpellier, France

Marc-André Gustcher
IUEM Domaines Océaniques, UMR 6538, CNRS, Université de Bretagne Occidental, Plouzané, France

Sabine Schmidt
EPOC, UMR 5805, CNRS, Université Bordeaux 1, Talence, France

Christian Beck
Laboratoire de Géodynamique des Chaînes Alpines, UMR 5025, CNRS, Université de Savoie, Le Bourget du Lac, France

Namik Çagatay, Ziyadin Çakir, Caner Imren, Kadir Eris, and Boris Natalin
Mining Faculty, General Geology Department, Istanbul Technical University (ITU), Maslak Istanbul, Turkey

Serdar Özalaybey and Leyla Tolun
Scientific and Technical Research Council of Turkey (TUBITAK) Marmara Research Center (MAM), Earth and Marine Sciences Research Institute, Kocaeli, Turkey

Irène Lefèvre
UMR 1572, CNRS, Laboratoire des Sciences du Climat et de l'Environnement, Gif-sur-Yvette, France

Leonardo Seeber
Lamont-Doherty Earth Observatory, Palisades, New York 10964, USA

Luca Gasperini
Istituto di Geologia Marina CNR-ISMAR, I-40129 Bologna, Italy

Claude Rangin
UMR 6535, CNRS, Collège de France, CEREGE, Aix-en-Provence, France

Omer Emre and Kerim Sarikavak
Geological Research Department, General Directorate of Mineral Research and Exploration (MTA), Balgat Ankara, 06520, Turkey

[1] Earthquake scarps associated with recent historical events have been found on the floor of the Sea of Marmara, along the North Anatolian Fault (NAF). The MARMARASCARPS cruise using an unmanned submersible (ROV) provides direct observations to study the fine-scale morphology and geology of those scarps, their distribution, and geometry. The observations are consistent with the diversity of fault mechanisms and the fault segmentation within the north Marmara extensional step-over, between the strike-slip Ganos and Izmit faults. Smaller strike-slip segments and pull-apart basins alternate within the main step-over, commonly combining strike-slip and extension. Rapid sedimentation rates of 1–3 mm/yr appear to compete with normal faulting components of up to 6 mm/yr at the pull-apart margins. In spite of the fast sedimentation rates the submarine scarps are preserved and accumulate relief. Sets of youthful earthquake scarps extend offshore from the Ganos and Izmit faults on land into the Sea of Marmara. Our observations suggest that they correspond to the submarine ruptures of the 1999 Izmit (Mw 7.4) and the 1912 Ganos (Ms 7.4) earthquakes. While the 1999 rupture ends at the immediate eastern entrance of the extensional Cinarcik Basin, the 1912 rupture appears to have crossed the Ganos restraining bend into the Sea of Marmara floor for 60 km with a right-lateral slip of 5 m, ending in the Central Basin step-over. From the Gulf of Saros to Marmara the total 1912 rupture length is probably about 140 km, not 50 km as previously thought. The direct observations of submarine scarps in Marmara are critical to defining barriers that have arrested past earthquakes as well as defining a possible segmentation of the contemporary state of loading. Incorporating the submarine scarp evidence modifies substantially our understanding of the current state of loading along the NAF next to Istanbul. Coulomb stress modeling shows a zone of maximum loading with at least 4–5 m of slip deficit encompassing the strike-slip segment 70 km long between the Cinarcik and Central Basins. That segment alone would be capable of generating a large-magnitude earthquake (Mw 7.2). Other segments in Marmara appear less loaded.

Components: 15,506 words, 12 figures, 1 video.

Keywords: continental deformation; earthquake scarps; Istanbul; Marmara; seismic hazard; submarine morphology.

Index Terms: 7223 Seismology: Earthquake interaction, forecasting, and prediction (1217, 1242); 7230 Seismology: Seismicity and tectonics (1207, 1217, 1240, 1242); 8110 Tectonophysics: Continental tectonics: general (0905)

Received 13 December 2004; **Revised** 2 March 2005; **Accepted** 24 March 2005; **Published** 24 June 2005.

Armijo, R., et al. (2005), Submarine fault scarps in the Sea of Marmara pull-apart (North Anatolian Fault): Implications for seismic hazard in Istanbul, *Geochem. Geophys. Geosyst.*, *6*, Q06009, doi:10.1029/2004GC000896.

1. Introduction

[2] The North Anatolian Fault (NAF) has almost entirely ruptured during a series of large destructive earthquakes in the past century. The sequence propagated 800 km westward between 1939 and 1999; an observation that has stimulated fundamental studies of fault interaction mechanics, stress transfer and earthquake rupture processes [*Toksoz et al.*, 1979; *Stein et al.*, 1997; *Nalbant et al.*, 1998; *Hubert-Ferrari et al.*, 2000; *Parsons et al.*, 2000]. Assessment of seismic hazard in the city of Istanbul, which is located near the western tip of the propagating sequence, is no independent issue. A uniform right-lateral strike-slip motion parallel to the Anatolia/Eurasia plate boundary may have facilitated the westward progression of earthquake ruptures along most of the eastern and central NAF. However, the Sea of Marmara region located westward appears as a major transtensional step-over of the NAF dominated by pull-apart tectonics and slip partitioning at a range of scales [*Armijo et al.*, 1999, 2002; *Flerit et al.*, 2003] (Figure 1). It is thus probable that crustal scale extensional strains and significant normal faulting add complexity to earthquake generation in the Marmara region. The study of the geomorphology of active faults on land appears worldwide as a good approach to unravel fault bends, slip partitioning and possible mechanical interactions between fault segments. Methods in tectonic morphology have greatly advanced over the last 25 years aided by satellite imagery, digital topography and modern techniques for dating, which allow quantitative measures [e.g., *Wallace*, 1981; *Hanks et al.*, 1984; *Armijo et al.*, 1986, 1989; *Peltzer et al.*, 1988; *Avouac et al.*, 1993; *Wesnousky and Jones*, 1994; *Meyer et al.*, 1998; *Hubert-Ferrari et al.*, 2002; *Van der*

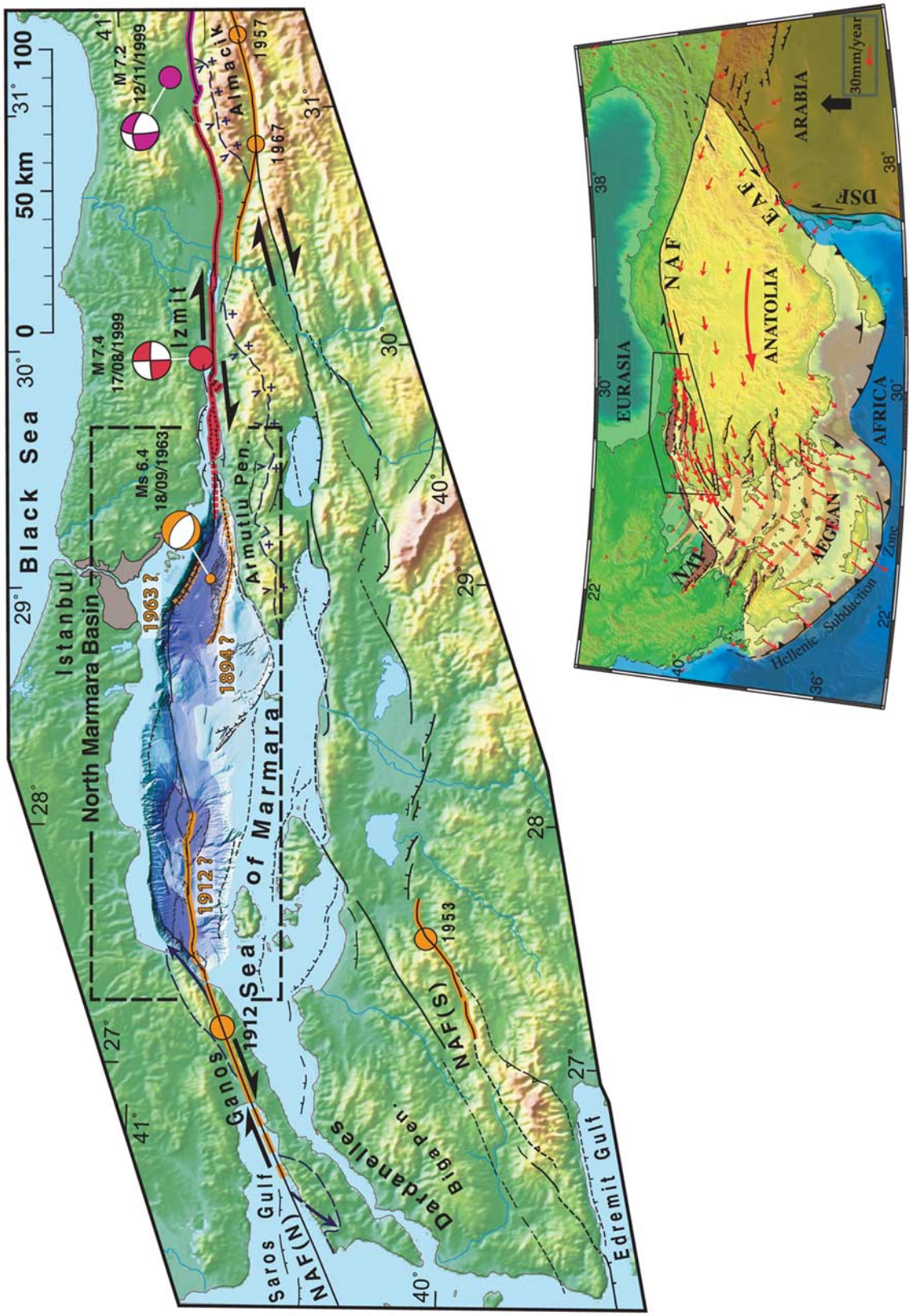
Black Sea
Istanbul
North Marmara Basin
Sea of Marmara
Armutlu Pen.
Izmit
Almacik
Ganos
Saros Gulf
NAF(N)
Bigha pen.
Dardanelles
Edremit Gulf
NAF(S)
M 7.2 12/11/1999
M 7.4 17/08/1999
Ms 6.4 18/09/1963
1912
1912 ?
1963 ?
1894 ?
1957
1967
1953
0 50 km 100
ARABIA
EURASIA
ANATOLIA
AFRICA
AEGEAN
DSF
NAF
EAF
Hellenic Subduction Zone
30mm/year

Figure 1

Woerd et al., 2002a; *Ritz et al.*, 2003; *Mériaux et al.*, 2004]. Here we adapt a similar approach for the submarine faults. The MARMARASCARPS cruise performed in 2002 collected high-resolution data to characterize the submarine morphology. These include microbathymetry, photo/video imagery and sediment sampling acquired with a ROV (Remotely Operated Vehicle), as well as coring and 3.5 kHz profiling with systematic coverage of the most prominent fault scarps in the northern Sea of Marmara. Together with data collected on other recent cruises we examine the morphology of submarine fault scarps and the shallow subbottom stratigraphy. Our aim is to characterize young earthquake ruptures and the morphological evolution of scarps, seeking to unravel first-order fault segmentation and significant geometrical barriers to rupture propagation. Some submarine breaks can be correlated with recent events or older historical earthquakes. Possible scenarios for the future earthquakes can be evaluated. One important question is to determine the present-day distribution of loading on the submarine segments in the northern Sea of Marmara and hence assess the nature of future events threatening Istanbul. We address this problem by describing the rupture length and possible slip distribution associated with recent earthquakes recorded by particularly well-preserved submarine scarps.

2. Tectonic Setting, Previous Work, and the New Data

2.1. Seismotectonic Background

[3] The Sea of Marmara is among the clearest examples of pull-apart basins in the world [*Armijo et al.*, 2002]. Here we focus on the Northern Branch of the NAF, which steps northwestward before entering the Aegean and which appears to concentrate most of the plate motion [*Straub et al.*, 1997; *Armijo et al.*, 1999; *McClusky et al.*, 2000; *Flerit et al.*, 2003]. The North Marmara basin is located by the conspicuous 70-km-wide step-over between two strike-slip faults, well-known on land, which have ruptured with purely right-lateral motion during recent earthquakes, both with similar magnitude (M 7.4) and clear surface rupture. One is the 1912 Ganos earthquake that ruptured the Dardanelles region to the west of the Marmara Sea; the second is the Izmit earthquake that ruptured in 1999 east of the Marmara Sea (Figure 1) [*Ambraseys and Finkel*, 1987; *Barka et al.*, 2002]. Long-term slip on the Izmit and Ganos faults puts the northern Marmara basin under an extensional regime that has caused significant overall subsidence [*Armijo et al.*, 2002; *Hirn et al.*, 2003; *Muller and Aydin*, 2005]. Short-term GPS-based models incorporating slip partitioning in the Sea of Marmara predict a right-lateral slip rate of about 18–20 mm/yr and extension of 8 mm/yr across the northern Marmara basin [*Flerit et al.*, 2003; *Armijo et al.*, 2003]. At a smaller scale the oblique fault system within the northern Marmara step-over is formed by smaller steps bounding three deep basins with lozenge shape and active subsidence that is stronger than in the rest of Marmara (depth ~1200 m: Tekirdag, Central and Cinarcik Basins) [*Barka and Kadinsky-Cade*, 1988; *Wong et al.*, 1995; *Armijo et al.*, 2002; *Okay et al.*, 1999, 2000; *Hirn et al.*, 2003; *Carton*, 2003].

[4] Not all authors subscribe the foregoing description. One class of alternative tectonic interpretations emphasizes that the extension in Marmara is associated with the widespread extension in the Aegean not with the localized pull-apart stretching [e.g., *Parke et al.*, 2002]. The new observations however do not support such views. The geology, the morphology and the GPS results at the regional scale exclude substantial Aegean extension as play-

Figure 1. The Sea of Marmara pull-apart and the submarine breaks found with ROV Victor 6000 (map redrawn from *Armijo et al.* [2002]). The NAF splays into a main northern branch (N) and a southern branch (S) that bypasses the pull-apart and accommodates much less motion. The North Marmara Basin is located by the step-over between the strike-slip Ganos and Izmit faults. The boxed area including the North Marmara Basin is enlarged in Figure 2, where names of smaller basins and step-overs are defined. Recent earthquake breaks and fault plane solutions of large earthquakes are outlined (fault plane solution for the 18 September 1963 event from *Taymaz et al.* [1991]; those for the 1999 events are from the USGS catalog). Submarine breaks found during the MARMARASCARPS cruise appear associated with recent historical earthquake ruptures (outlined with colors and labeled by date of occurrence): (1) the eastern extension of the 1912 (Ms 7.4) Ganos earthquake; (2) the western end of the 1999 (Mw 7.4) Izmit earthquake; (3) the 1963 (Ms 6.4) Yalova earthquake; (4) the 1894 (M~7) Cinarcik earthquake. However, no young break was found between the Central Basin and the Cinarcik Basin (names labeled in Figure 2). Geologic markers (dashed blue) are those used for restoring slip in Marmara as discussed by *Armijo et al.* [1999]. The inset shows the tectonic framework. NAF, North Anatolian Fault; EAF, East Anatolian fault; DSF, Dead Sea Fault; NAT, North Aegean Trough. GPS velocity vectors (in red, referenced to a fixed Eurasia) from *McClusky et al.* [2000].

ing a significant role in the finite deformation of the Marmara Sea region [*Armijo et al.*, 2002; *Flerit et al.*, 2003, 2004].

[5] Another class of interpretations dismisses currently active extension, proposing alternatively pure strike-slip on a single throughgoing fault across Marmara [e.g., *Le Pichon et al.*, 2001, 2003]. Different geometries with increasing complexity have been offered successively for this hypothetical fault [*Le Pichon et al.*, 1999, 2000, 2001; *Imren et al.*, 2001]. It has also been claimed that the strike-slip faulting would have crossed the region recently (~200 ka), coevally with a major tectonic reorganization in the Sea of Marmara, due to a very young inception of the NAF. Hence motion on the NAF in this region should have produced only minor total offset (4 km of right-lateral offset) [*Le Pichon et al.*, 2003; *Demirbag et al.*, 2003; *Rangin et al.*, 2004; *Sengör et al.*, 2004]. The growing body of evidence gives little support to these views. First, large right-lateral offsets across purely strike-slip segments of the NAF are well identified on land on both sides of the Sea of Marmara pull-apart [*Armijo et al.*, 1999, 2000]. Offsets of geological structures and morphologic markers amount to tens of kilometers (totaling 85 km ± 10 km), which must have taken no less than 4–5 Myr to form [*Westaway*, 1994; *Schindler*, 1998; *Armijo et al.*, 1999, 2002]. Second, recent studies of the structure in the northern Marmara basin using independent approaches (fault mapping from bathymetry [*Armijo et al.*, 2002], high-resolution multichannel seismic reflection profiles with dense coverage [*Hirn et al.*, 2003; *Carton*, 2003] and mechanical modeling [*Muller and Aydin*, 2005] show consistently that steady subsidence, fault segmentation and development of pull-apart basins have been the prevalent processes for 1 Myr or more, with no significant tectonic change during that time period. Studies of active fault morphology and geology in the Gulf of Saros, the Gulf of Izmit and the Ganos region are also consistent with the simple pull-apart evolution in Marmara [*McNeill et al.*, 2004; *Polonia et al.*, 2004; *Seeber et al.*, 2004].

[6] In keeping with the interpretation of the pure strike-slip fault proposed by *Le Pichon et al.* [1999], *Meade et al.* [2002] and *Le Pichon et al.* [2003] deduce kinematic models defining a rigid "Marmara block." While producing a good fit to GPS vectors those models appear kinematically inappropriate because the pure strike-slip motion they obtain within the extensional Marmara step-over produces a large compression across the strike-slip Izmit fault (up to 5–6 mm/yr), which is inconsistent with the well-known motion of that fault and with the best constrained earthquake mechanism available for the region (1999 Izmit earthquake; Mw 7.4). Clearly the GPS data alone do not provide a definite test. It has been shown that models producing a good fit to the GPS vectors, but also incorporating clear kinematic constraints in the Marmara region require pull-apart extension and slip partitioning [*Flerit et al.*, 2003].

[7] The single throughgoing fault hypothesis has also been used to predict full rupture of the north Marmara submarine fault system during a future large earthquake [*Le Pichon et al.*, 1999, 2000, 2003; *Sengör et al.*, 2004]. We deal with this critical issue later.

[8] A simple observation is that the 1912 Ganos and the 1999 Izmit earthquakes bracket a 160-km-long stretch of interconnected submarine fault segments stepping across the northern Marmara step-over, combining normal and right-lateral motion [*Armijo et al.*, 2002]. It has previously been assumed that this submarine stretch has not ruptured during the 20th century (Figure 1) and so probably tectonic loading in the north Marmara region would be uniformly high [*Hubert-Ferrari et al.*, 2000]. However, the ruptures of the 1912 and 1999 earthquakes were both seen to extend into the Sea of Marmara. For the Izmit earthquake its submarine western end is reasonably well resolved with space geodesy, especially the SAR interferometry, which documents the far-field surface deformation in the land areas surrounding the Gulf of Izmit. The rupture appears to have propagated no more than 30 km west of the Hersek peninsula into the Sea of Marmara (Figure 1) with slip tapering from 2 m to zero [*Çakir et al.*, 2003]. For the 1912 Ganos earthquake the direct observations of the rupture on land are reported mainly by *Mihailovich* [1927]. Later revisions [*Ambraseys and Finkel*, 1987; *Altunel et al.*, 2004] using damage distribution and field observations suggest that the rupture propagated well into the Sea of Marmara, although with unknown extent. Indeed, it has been proposed that large historical earthquakes (1509, 1719, May 1766, August 1766, 1894) ruptured totally or partially segments under the northern Sea of Marmara [*Ambraseys and Finkel*, 1991, 1995; *Ambraseys and Jackson*, 2000; *Parsons*, 2004; *Rockwell et al.*, 2001]. Tangible evidence of their submarine rupture geometry and location

however is lacking. It is also generally assumed that the 18th century sequence ruptured entirely this part of the NAF and so tectonic loading has been accumulating since then, unrelieved by significant rupture in the north Marmara basin [*Hubert-Ferrari et al.*, 2000; *Parsons et al.*, 2000; *Le Pichon et al.*, 2003; *Parsons*, 2004]. This view has been questioned by *Ambraseys and Jackson* [2000], who reassessed possible locations of the large historical earthquakes and suggest a much longer quiescence in central and western Marmara. Our direct observations of the Sea of Marmara floor allow us to address some of these issues, especially the extent of submarine rupture in 1912.

2.2. MARMARASCARPS Cruise Data: Key Results

[9] During the MARMARASCARPS cruise the unmanned submersible ROV Victor 6000 and the oceanographic vessel Atalante were used in September-October 2002 to perform a high-resolution, high-precision bathymetric survey (microbathymetry) of the main submarine faults in the northern Sea of Marmara. The ROV was operated with a Seabat 8101 multibeam sounder to survey faults over a total length of about 300 km with an average horizontal resolution of 0.5 m and a vertical accuracy of 10 cm, using a high-precision submarine navigation system (less than 10 m of uncertainty) based on a DGPS positioning of the vessel. Exploration at low altitude over the sea bottom (2 m) was made in specific sites to make direct visual observations of the fault breaks. The ROV landed to sample 35-cm-long cores into the disturbed sediment in the immediate vicinity of scarps. Samples of authigenic carbonate crusts where also collected near cold seeps and vents found often associated with the scarps. Appropriate projectors and photo/video cameras were used extensively (key areas are shown in a video supplement that is available as auxiliary material)[1]. To characterize the stratigraphic environment and the sedimentary evolution of the deep Marmara basins, an extensive survey totaling 600 km of profiles with a 3.5 kHz sediment penetrator across the main deep basins (Tekirdag Basin, Central Basin and Cinarcik Basin) was undertaken. A complementary sampling of the seafloor sedimentary cover close to the faults with a 5-m-long gravity corer was also performed.

[10] For the present study we use complementary data from other cruises led by a French-Turkish collaboration program (Program on the study of seismic hazard in Istanbul and Sea of Marmara region). These include (1) a full coverage of the north Marmara basin with EM300 multibeam bathymetry (30 m resolution) and side-scan imagery from cruise MARMARA (performed in 2000), and (2) results from long sediment cores (35 m long) and calibrated ^{14}C ages of wood fragments from cruise MARMACORE (performed in 2001).

[11] During the MARMARASCARPS cruise clear morphologic evidence of recent faulting activity was found along several segments of the northern Marmara fault system. Along some of the faults, fine, outstandingly well-preserved scarps were discovered, probably associated with recent earthquake breaks. The key results are identified in Figure 1: (1) An outstanding break extends offshore eastward of the Ganos fault, between that fault and the Central Basin. (2) A very fresh break is seen where the Izmit fault enters westward into the Cinarcik Basin. It corresponds very probably to the underwater extension of the 1999 Izmit earthquake rupture [*Çakir et al.*, 2003; *Wright et al.*, 2001; *Reilinger et al.*, 2000; *Feigl et al.*, 2002; *Karabulut et al.*, 2002]. (3) Small fresh breaks cut along the NE edge of the Cinarcik Basin over several kilometers. They can be associated tentatively with the Ms 6.4 1963 earthquake [*Ambraseys*, 1988; *Taymaz et al.*, 1991]. (4) The fault scarp at the SW edge of the Cinarcik Basin corresponds to a sharp, steep contact between bedrock and young sediments. It is seemingly the most likely candidate for the M$\sim$7 1894 earthquake rupture [*Parsons*, 2004]. (5) No young break could be detected between the Central Basin and the Cinarcik Basin.

[12] In the following sections we present and discuss selections of the microbathymetry and of the 3.5 kHz profiles, aimed at focusing on the set of earthquake scarps found in western Marmara (Figure 2) (A full description and discussion of the data (microbathymetry, 3.5 kHz profiles and cores), particularly on the other scarps found during the MARMARASCARPS cruise, will be purpose of future papers by N. Pondard, G. Ucarkus, B. Mercier de Lépinay, and S. Schmidt)). Those scarps are covered systematically, almost continuously with the high-resolution data. They cross three local tectonic environments (transtension,

[1]Supporting material is available via Web browser or via Anonymous FTP from ftp://ftp.agu.org/apend/" (Username = "anonymous", Password = "guest"). Subdirectories in the ftp site are arranged by journal and paper number. Information on searching and submitting electronic supplements is found at http://www.agu.org/pubs/esupp_ about.html.

nearly pure strike-slip and transpression) where different morphologic features have formed. The selected sites are described following that logic (from the Central Basin to the Western High and the eastern Tekirdag Basin, then the western Tekirdag Basin), which is simply to proceed from east to west. Similar to elsewhere on land, the submarine scarp morphology in Marmara develops as a result of accumulation of earthquake slip during the late Quaternary, with the recent, readily visible earthquake scarps corresponding to the last increments. Consequently the earthquake scarps are described along with their combined morphologic/geologic context.

3. Submarine Scarps in NW Marmara

3.1. Morphology and Geology of the Central Basin Pull-Apart: Rates of Sedimentation and Normal Faulting

[13] The Central Basin (Figure 2) appears as a clear nested pull-apart structure with rift-in-rift cross section, which is seen both in its morphologic expression [*Armijo et al.*, 2002] and in its deep structure as determined by well-resolved seismic sections [*Hirn et al.*, 2003].

[14] In map view (Figure 2), the edges of the outer pull-apart are marked by large boundary faults striking NW-SE at the base of 1-km-high escarpments, which appear eroded and drained by submarine valleys. These faults embrace the flat floor of the Central Basin where sediments accumulate. The map (Figure 2) also shows the inner pull-apart with typical lozenge shape between two strike-slip segments (to the E and W), which is bounded (to the NE and SW) by sharp normal fault scarps that offset the flat bottom of the basin. The larger normal fault scarps across the bottom strike mostly NW-SE and are formed by series of smaller (1- to 3-km-long) left-stepping, en echelon segments, which attest to the nonetheless dominant, right-lateral motion across the overall fault zone. In cross section (Figure 3), the structure of the 7-km-wide inner pull-apart can be appreciated; the lower inner floor appears flanked by the inner boundary faults and across them, by somewhat higher, flat shoulders.

[15] The subsidence of the inner floor and the sediment distribution are both controlled by continuing activity of the inner boundary faults. That dependence is readily seen in the profiles obtained with the 3.5 kHz sediment penetrator, which illuminates and resolves with good accuracy the structure down to 70 ms, or ~50 m depth below the seafloor (Figure 3). The 3.5 kHz profile shown is correlated with cores 31 and 29, which provide the complete record of pelagic and turbiditic sediments deposited from the late Pleistocene to the present [*Mercier de Lépinay et al.*, 2003; *Beck et al.*, 2003]. In the Sea of Marmara the late Pleistocene-Holocene transition includes the effects of the global postglacial sea level rise. A lacustrine environment isolated from both the Black Sea and the Aegean prevailed during the late Pleistocene glacial low sea level. This stage is followed by a sharp marine transgression [*Çagatay et al.*, 2000, 2003; *Mercier de Lépinay et al.*, 2003; *Polonia et al.*, 2004]. The cores in the Central Basin and the correlation in Figure 3 establish that this marine transgression has occurred after ~14 ka. About 35 m of marine sediments have accumulated since the transgression over the inner floor of the Central Basin and only 10 m over its SW shoulder (south of the boundary fault), at minimum average sedimentation rates of 2.5 mm/yr and 0.7 mm/yr, respectively. A similar feature with less offset is seen at the NE edge of the inner floor (Figures 2 and 3). Thus sedimentation rates found in the deep bottom of the Central Basin (and in the other deep basins of Marmara; see *Mercier de Lépinay et al.* [2003]) are substantially faster than sedimentation rates previously found in shallower parts of the Marmara basin ($\leq$0.3–0.5 mm/yr in the shallow shelves at depths $\leq$100 m; 0.1–0.2 mm/yr at intermediate depths of 300–700 m [*Çagatay et al.*, 2000]).

[16] The differences in sediment thickness in the floor of the Central Basin are sharp. They must be accounted for by vertical motion across faults with large normal component, especially across the larger inner boundary faults, which have significant continuity in map view (Figure 2). Stratigraphic offsets indicate that these larger faults are very active (2–6 mm/yr throw rate) and that they have created sharp scarps in the bathymetry. Conversely,

Figure 2. Bathymetry and active faults in the North Marmara Basin. Top panel identifies local names. Cores 29 and 31 are located within and south of the inner pull-apart in the Central Basin. Bottom panel (redrawn from *Armijo et al.* [2002]) identifies the trace of active faults with color outlines and dates indicating recent earthquake breaks. Small red boxes and numbers locate detailed observations of seafloor breaks described in the text and the following figures. The line across the Central Basin locates the section in Figure 3.

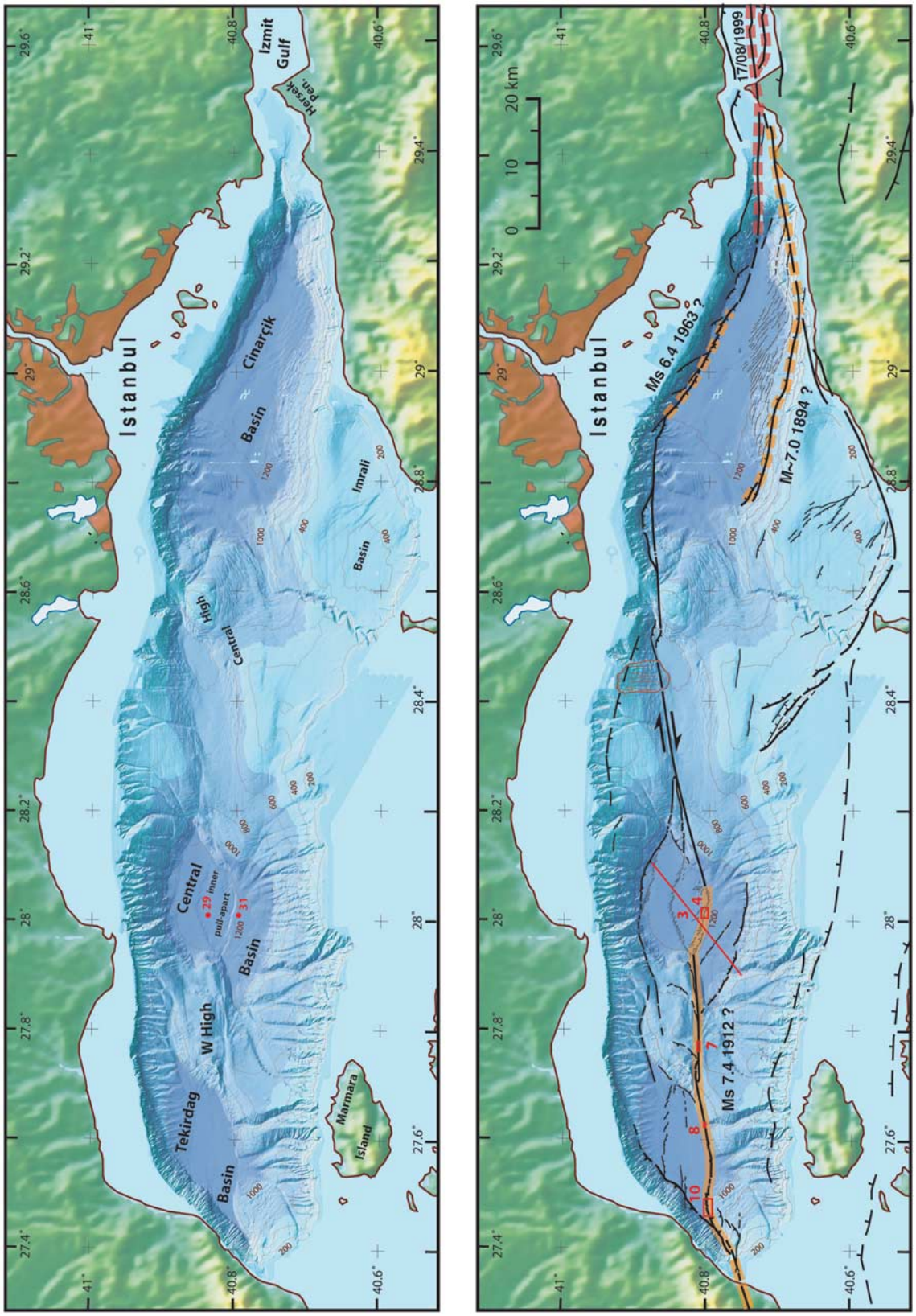
Istanbul
Izmit Gulf
Herzek Pen.
Cinarçik Basin
Imrali Basin
Central High
Central Basin
W High
Tekirdag Basin
Marmara Island
pull-apart
Istanbul
Ms 6.4 1963 ?
M~7.0 1894 ?
17/08/1999
Ms 7.4 1912 ?
0 10 20 km

Figure 2

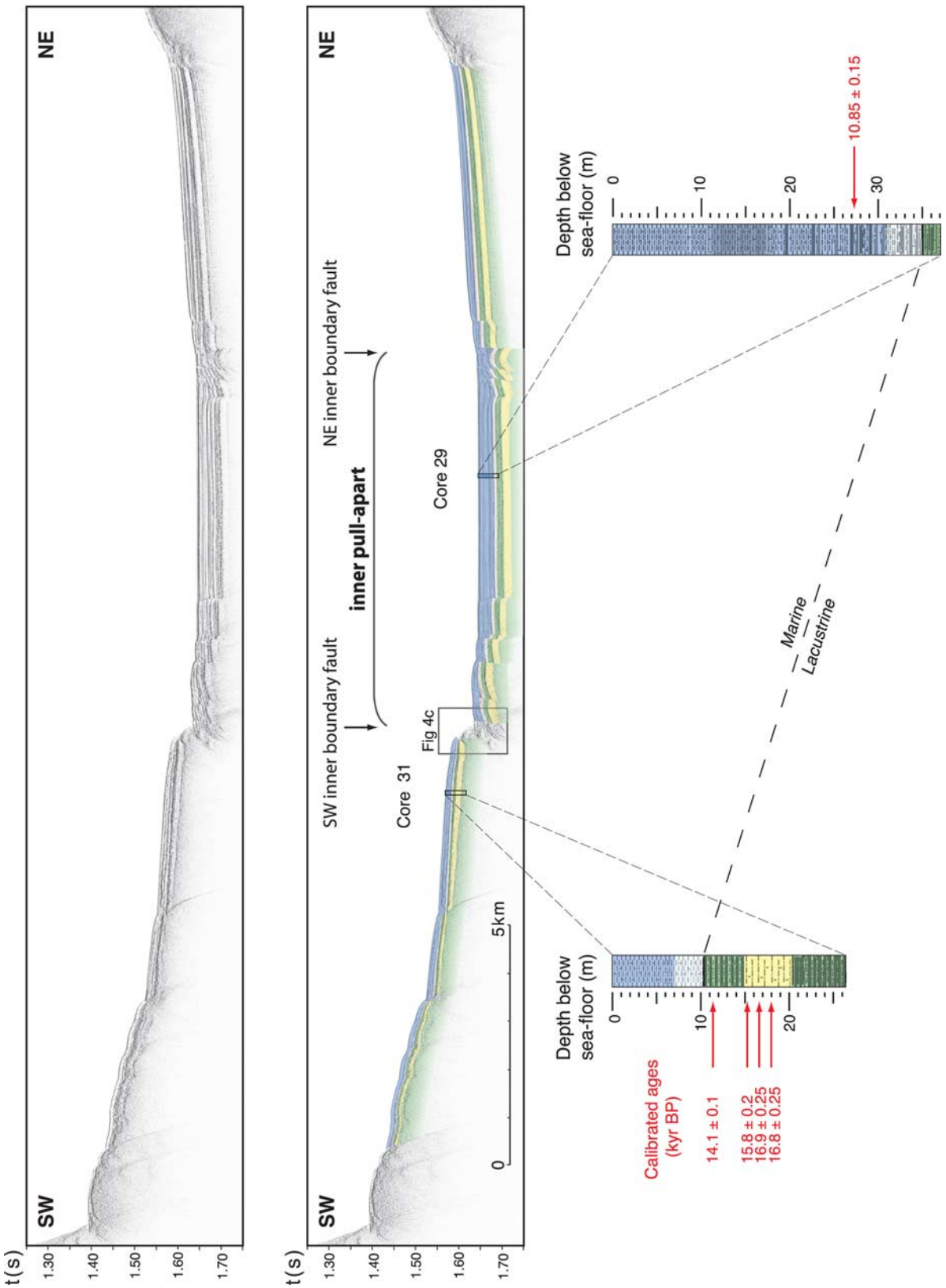
NE
SW
t(s)
1.30
1.40
1.50
1.60
1.70
NE
SW
t(s)
1.30
1.40
1.50
1.60
1.70
NE inner boundary fault
inner pull-apart
SW inner boundary fault
Core 29
Core 31
Fig 4c
0
5km
Depth below sea-floor (m)
0
10
20
30
10.85 ± 0.15
Marine
Lacustrine
Depth below sea-floor (m)
0
10
20
Calibrated ages (kyr BP)
14.1 ± 0.1
15.8 ± 0.2
16.9 ± 0.25
16.8 ± 0.25

Figure 3

smaller secondary faults with less continuity in map view have less stratigraphic offset, less or none morphologic expression and thus appear less active ($\leq$1 mm/yr throw rate). So vertical motion associated with normal faulting and sediment accumulation are the basic competing processes explaining both the late Pleistocene-Holocene stratigraphic variations and the morphology of the Central Basin floor.

[17] The foregoing geological and morphological observations suggest that the fast normal fault throw rates induce fast subsidence and sedimentation rates in the deep basins of Marmara. Those rates are both particularly fast, consistent with the high rates of strike slip and pull-apart extension deduced for the north Marmara fault system at larger scale [*Straub et al.*, 1997; *Armijo et al.*, 2002; *Flerit et al.*, 2003, 2004; *Muller and Aydin*, 2005].

3.2. Origin of Submarine Scarps and the Glacial-Interglacial Transition

[18] The growth of the submarine scarps under competing normal faulting and sedimentation processes is important to understand the submarine scarp preservation. It is clear that offsets of the late Pleistocene-Holocene stratigraphy increase with depth for any of the faults seen in the 3.5 kHz profiles (Figure 3), but the two inner boundary faults are well identified in multichannel seismic profiles to depths of some kilometers (3–5 sec or about 3–5 km), with significant offsets across them (hundreds of meters) [*Imren et al.*, 2001; *Hirn et al.*, 2003]. This suggests that these faults are long-lived structures that are much older than the recent sediments seen in Figure 3. This implies that the height of the scarps across the seafloor is modest when compared with the duration of the faulting. However, as the recent pile of sediments was deposited, the scarps were systematically growing higher, suggesting that at some "origin" time in the past, rapid sedimentation filled in a faulted morphology to produce a more recent "initial" surface. Some balance between competing normal faulting and sediment accumulation must determine the initial surface and the origin time for this process. Thus scarp-forming processes under submarine conditions appear similar to scarp-forming processes on land, where abrupt changes in morphologic rates and climatic changes are intimately tied together. This link has been well established in diverse continental environments, particularly for active fault scarps that have formed since the last deglaciation and after the setting-up of the present interglacial conditions (i.e., the Holocene [e.g., *Armijo et al.*, 1986, 1989, 1991, 1992; *Peltzer et al.*, 1988; *Meyer et al.*, 1998; *Van der Woerd et al.*, 2001, 2002b; *Benedetti et al.*, 2002, 2003]).

[19] Our observations in the Sea of Marmara suggest that the young submarine scarps like those atop the boundary faults of the central pull-apart formed after a period of very rapid sedimentation during deglaciation (sedimentation rate $\geq$5 mm/yr), which included thick catastrophic events (homogenites; see *Beck et al.* [2003]). The rapid sedimentation has probably concealed previous tectonic topography and leveled the Central Basin seafloor to a flat surface. After that initial stage of leveling, the marine transgression and the interglacial conditions have diminished sedimentation rates (to the present-day ones). These new conditions with average sedimentation rates lower than vertical slip rates are favorable for earthquake scarps to emerge from sediments and to remain un-submerged by subsequent sedimentation before the next earthquake slip has occurred. In this way scarps associated with the faster faults can progressively accumulate topography with subsequent earthquake faulting and with time. Figure 3 shows examples of faults with different slip rate and so, with different capacity to form scarps.

3.3. Relation Between Cumulative and Individual Normal-Fault Scarps in the Central Basin: Slip Contributed by the Last Scarp-Forming Event

[20] A cumulative scarp 50 m high has formed at the SW boundary fault of the inner pull-apart, where the late Pleistocene-Holocene sediment pile is exposed to erosion (box in Figure 3, middle panel, Figures 4 and 5a). Figures 4a and 4b show the one-to-one correspondence of small-scale morphologic features mapped with multibeam microbathymetry and seen on the side-scan sonar image.

Figure 3. Section across Central Basin. Upper Pleistocene and Holocene sedimentary pile as defined by the high-resolution 3.5 kHz profile (top two panels; data without and with interpretation) and enlarged core logs (bottom panel; cores 31 and 29 from MARMACORE cruise, 26 and 37 m long, respectively) with sediment description and ^{14}C calibrated age constraints (dated wood fragments). Faults with normal slip at edges of inner pull-apart are readily seen. The box in the middle panel locates Figure 4c.

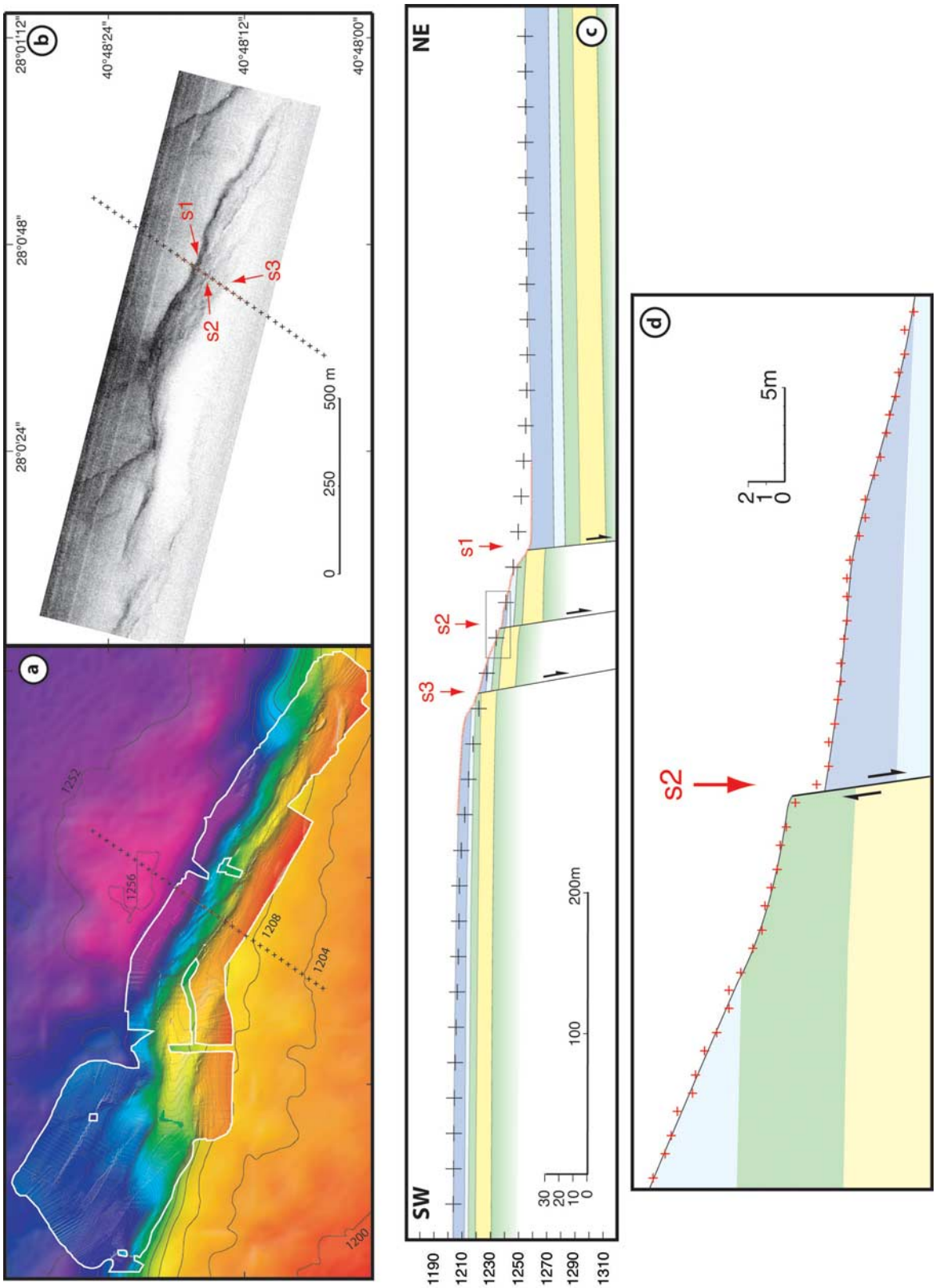
a
b
c
d
28°01'12"
28°0'48"
28°0'24"
40°48'24"
40°48'12"
40°48'00"
s1
s2
s3
0
250
500 m
1252
1256
1208
1204
1200
NE
SW
1190
1210
1230
1250
1270
1290
1310
100
200m
30
20
10
0
5m
2
1
0

Figure 4

The two images reveal the fine details of the cumulative scarp including secondary branches, echelons, horse-tail terminations, etc., comparable to active trans-tensional fault scarps commonly observed on land, under prevailing erosional conditions. Slope-degrading processes such as gravity collapse, sliding, talus creep and overall sediment transport appear to prevail over sediment deposition across the whole 50-m-high cumulative scarp (over a width of about 100 m; Figure 4c). Such conditions can be readily appreciated in the sea-bottom pictures (Figure 5).

[21] The most striking feature defined in both the side-scan sonar and the microbathymetry is the occurrence of small-scale, sharp, steep scarps that lacerate the larger cumulative scarp (Figures 4a, 4b, and 5). The small-scale scarps (called hereafter individual scarps) cut obliquely across the slopes of the cumulative scarps, with a finer en echelon branching structure. The steepness and the sharpness of the individual scarps suggest that they correspond to the latest scarp-forming increments. Those steep increments are also seen directly in the imagery taken at the sea bottom (see Figure 5b). The individual scarps seen in the Central Basin appear comparable to recent earthquake scarps observed elsewhere on land. Some striking similarities can be appreciated in Figure 6.

[22] Nevertheless it is difficult to discern strictly the amount of slip associated with the last scarp-forming event only. An "individual" scarp could result from more than one event. Closer examination of microbathymetry profiles across individual scarps and of the direct bottom imagery allows us to estimate, within error, the slip attributable to the last scarp-forming event. Three individual en echelon scarps (marked with arrows labeled s1, s2 and s3 in the side-scan sonar image, Figure 4b) can be appreciated as slope breaks over three secondary faults in the microbathymetry profile and the interpreted section (Figure 4c). The enlargement of the microbathymetry data shows that scarp s2 is about 1–2 m high (Figure 4d) with a free face that occupies a large part of it. This feature is seen in the photo imagery of this scarp (s2) and other correlatable scarps (Figures 5b, 5c, and 5d). Thus the last scarp-forming event at s2 appears to have contributed an incremental throw of 1–2 m. Similarly, s3 would have contributed a throw of 0.5–1 m during the last scarp-forming event.

[23] Free faces are easier to discern and incremental throws easier to determine for the two upper individual scarps (s2 and s3), where the slope of the cumulative scarp is shallower, than for scarp s1 that is located at the very base of the cumulative scarp, where its slope is steeper. For basal scarp s1, which is generally the largest of individual scarps in any section across the SW boundary fault, the incremental throw corresponding to the last scarp-forming event could be similar (or larger) to that determined for scarp s2, but this assessment remains very uncertain. Indeed it is difficult to estimate with accuracy the total incremental throw corresponding to the last scarp-forming event, by summing the contributions of s1, s2 and s3 along the section presented in Figure 4c. With caution we estimate for the last event a total incremental throw of at least 2 m and possibly not much more than 4 m.

[24] Individual scarps with the same morphologic characteristics and bearing free faces of similar size were followed visually with the ROV (video cameras) for many hundred meters along strike, in this segment and the other segments of the SW boundary fault. The microbathymetry survey and the side-scan data suggest this set of incremental scarps with significant normal slip is continuous all along the whole SW boundary fault of the inner pull-apart, for a total length of about 8 km (Figure 2). We deduce that the SW boundary fault has ruptured entirely during this event possibly with an average throw of no less than 2–4 m. No

Figure 4. Morphology of a fault segment in the Central Basin. The 1.5-km-long segment shown has significant normal component of slip. It is one of the north-dipping segments forming the left-stepping en echelon fault system at the SW edge of the inner pull-apart (Figures 2 and 3). (a) Bathymetry. The map combines background EM300 data (30 m resolution, 1 m vertical accuracy) with microbathymetry (white outline) collected near bottom with Seabat 8101 mounted on ROV Victor 6000 (0.5 m resolution, 0.1 m vertical accuracy). Contours every 1 m. Black and smaller red crosses indicate profile location. (b) Side-scan sonar image. Profile location is indicated for comparison. Arrowed s1, s2, and s3 identify individual scarps. (c) Section constructed with combined bathymetry and stratigraphy (3.5 kHz and core data; colors as in Figure 3). The ROV microbathymetry data (small red crosses) resolves details of the scarp morphology (not resolved with the background bathymetry; black crosses). The 50-m-high cumulative scarp is formed of 3 steps, which are marked by individual scarps (s1, s2, and s3; identified in the side-scan sonar image). Stratigraphy is not resolved in fault blocks between s1 and s2. (d) Enlargement of individual scarp s2. The 1- to 2-m-high free face corresponds to the last fault rupture. Stratigraphy is schematic. No vertical exaggeration.

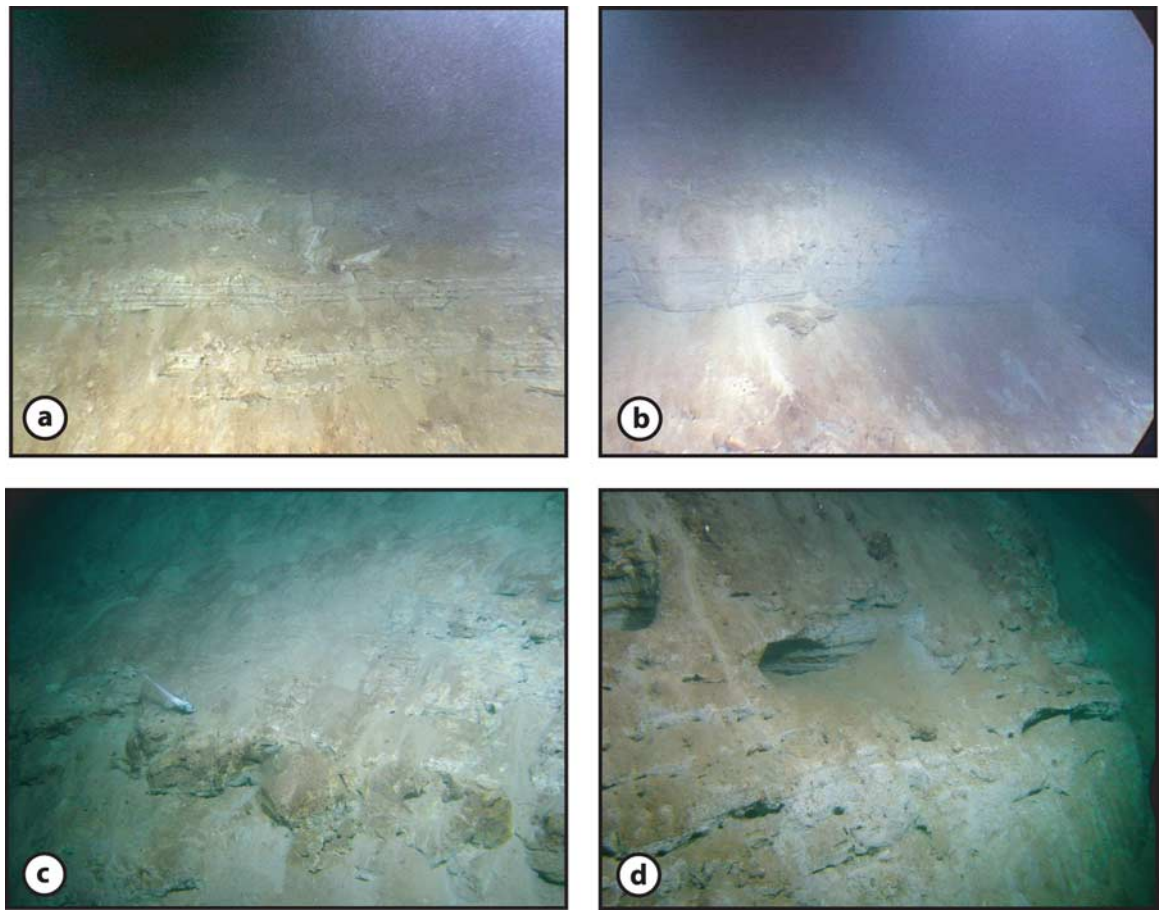

Figure 5. Sea-bottom pictures of dominantly normal fault scarps in the Central Basin (corresponding to features in Figure 4). (a) View of cumulative scarp exposing horizontal strata of Holocene and upper Pleistocene age. Total visible height is ~20 m. View to south. (b) Individual scarp (correlatable with s2 in Figure 4) exposes 1- to 2-m-high free face (last fault rupture) between eroded convex surface at its top and sediment talus at its base. View to SW. (c) Top of individual scarp (s2) exposes fine-grained, fine-layered, whitish (lacustrine?) strata atop 15-cm-thick coarser turbidite. Fish (10 cm long) gives scale. View to south. (d) Top of scarp s2 grades downward into steeper free face exposing normal fault plane possibly with purely dip-slip slickensides (bottom right corner), which suggests slip partitioning. However, it was not possible for us to determine precisely how strike-slip and normal slip are partitioned across the SW edge of the inner pull-apart. Visible height of free face is 0.6 m. View to SW.

lateral slip can be measured from the morphology of scarps, although the orientation of the overall en echelon structure requires a significant component of right-lateral slip, possibly of the same order as the normal throw.

3.4. Strike-Slip Scarps and Last Event Slip Determined Across the Western High

[25] A very linear 20-km-long strike-slip fault segment links the inner SW boundary fault of the Central Basin inner pull-apart with the fault at the southern edge of the Tekirdag Basin (Figure 2). The extracts of the microbathymetry and of the side-scan sonar imagery in Figure 7 cover the shallowest area crossed by the fault, at about 650–670 m depth. As for the Central Basin, the two data sets show a one-to-one correspondence of the fine-scale features defining the young fault scarps. At this smaller scale the fault trace is still very linear, but with a slight sinuosity apparently associated with the smaller-scale segmentation. Pressure ridges and pull-apart ponds alternate at segment ends or at slight fault bends. The dimensions of such features (10–150 m in length; 10–50 m in width, respectively along and across strike, associated with several meters of vertical relief) indicate that they may have resulted from many events. The microbathymetry also shows that opposite north- and south-facing scarps alternate

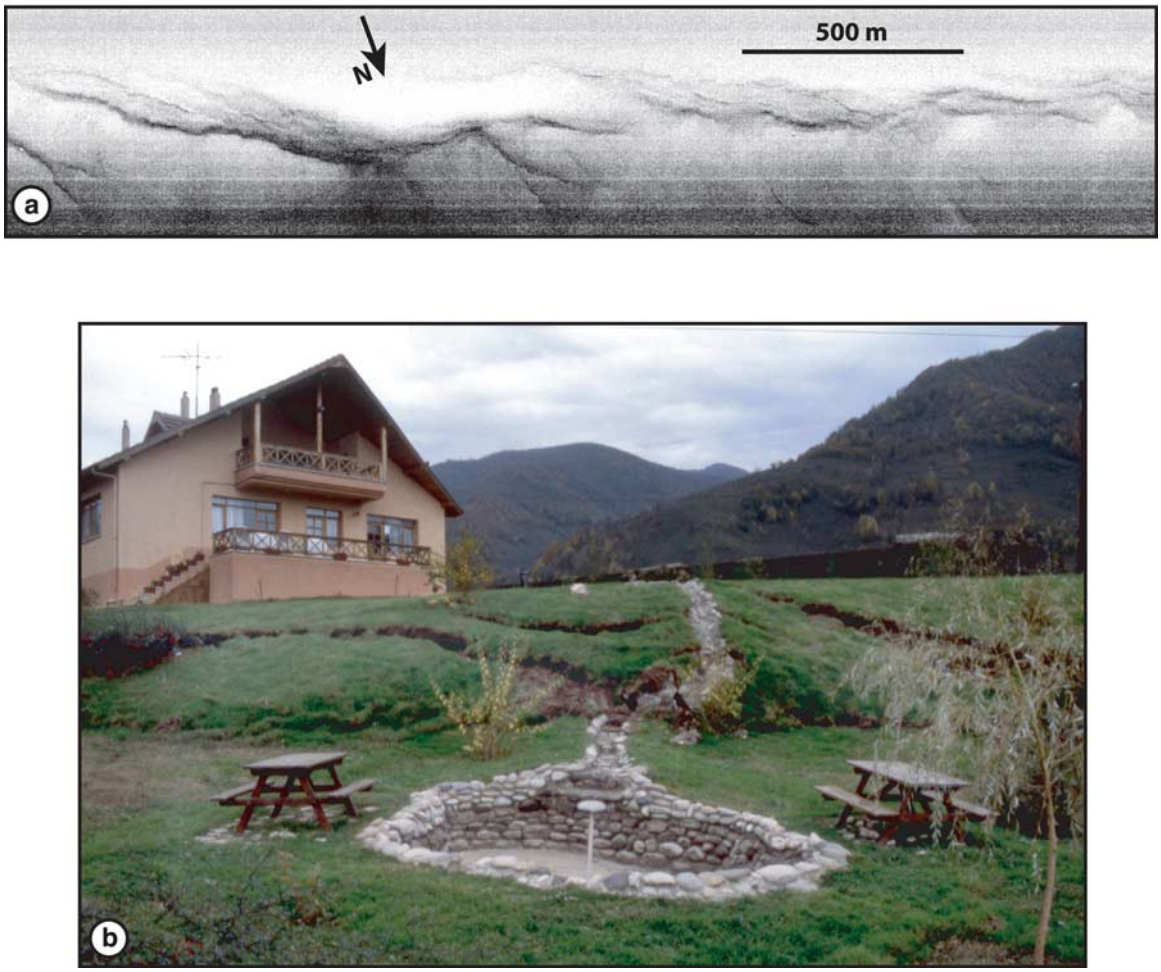

Figure 6. Submarine scarps in the Central Basin compared with similar scarps on land near Eften lake extensional step-over. (a) Side-scan sonar image (illuminated from the SE) of large en echelon scarps with normal and right-lateral strike-slip components on the SW boundary fault of the inner Central Basin pull-apart (compare with Figures 4 and 5). (b) Scarps with similar features but substantially smaller near the western termination of the 12 November 1999 Duzce earthquake rupture (Mw 7.2). Individual scarps with free faces 20–50 cm high associated with the Duzce earthquake lacerate obliquely a cumulative normal fault scarp 4 m high. The inlet providing water to the pool has been right-laterally offset 1.5 m across individual fault scarp at the very base of the cumulative scarp. Total normal and strike offsets reached 4 m in 1999 in the Eften area [*Akyüz et al.*, 2002].

along strike, attesting that there is no systematic vertical offset of the morphology; thus the prevailing motion across the fault is strike-slip.

[26] The most outstanding feature is the continuity and the linearity of a set of scarps that are in many places less than 0.5 m high (less than one contour line in the microbathymetry map; Figure 7). This set of continuous individual scarps comes into sight in the microbathymetry as a sharp cut made into the soft sediments covering the smooth topography of the Western High. Visual inspection with the ROV proved that the small-scale scarps are mantled with a drape of soft pelagic sediments and

Figure 7. Morphology of EW-striking, purely strike-slip fault scarps across the Western High. (a) Microbathymetry (top) and corresponding side-scan sonar image (bottom) show smooth sea-bottom morphology disrupted by a sharp, continuous break along the linear fault trace (outlined by red arrows). Disruption of morphology occurs at various scales with opposite north- and south-facing vertical offsets suggesting prevailing strike-slip. Pressure ridges and pull-apart ponds can be seen (examples identified). Contours each 0.5 m. (b) Enlargement of shallowest area (box in Figure 7a), where sea-bottom landforms are clearly offset laterally. (c) Restoring offsets of individual scarp requires 6 ± 1 m of right-lateral slip, which could result mostly from rupture of a large earthquake.

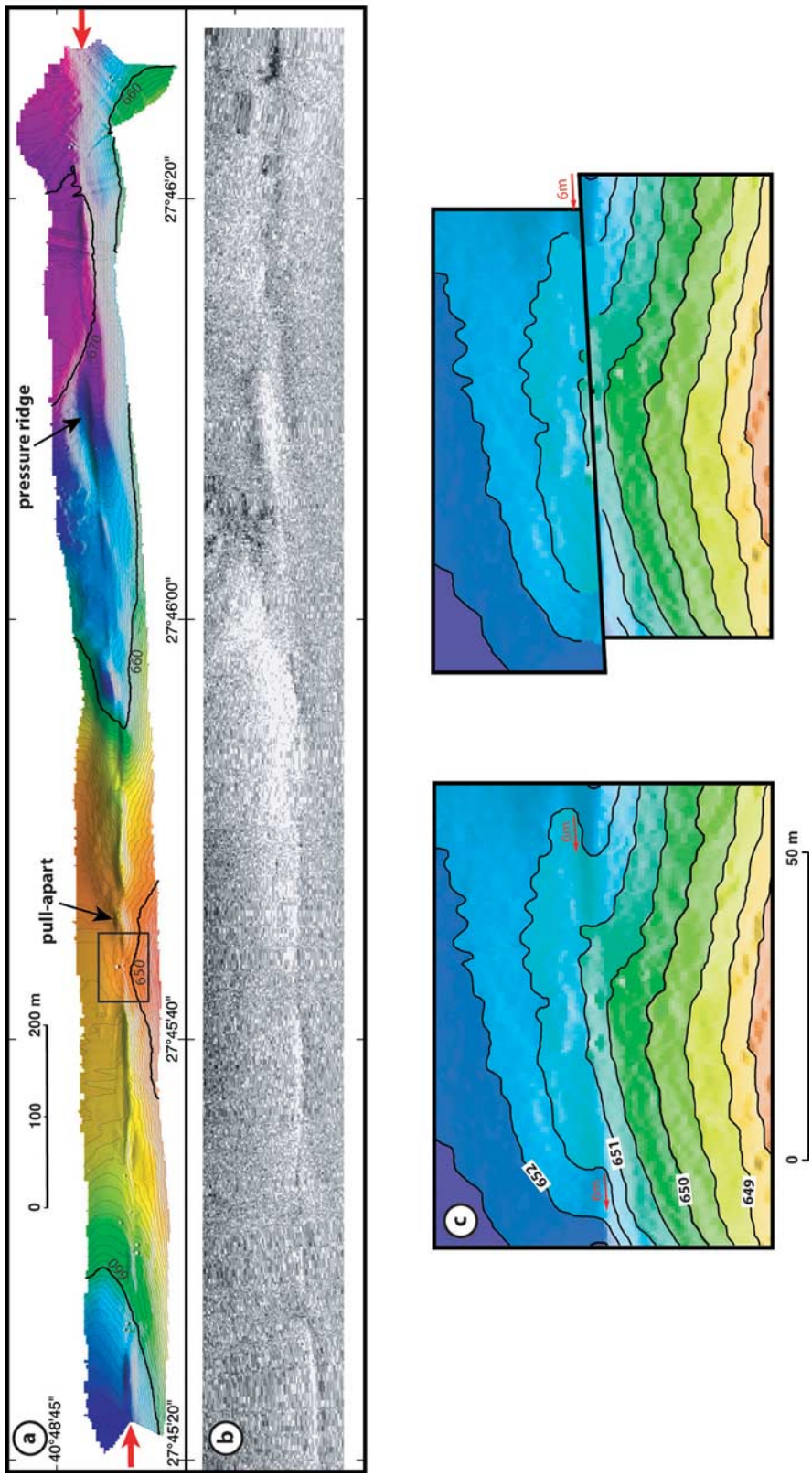
a
b
c
pressure ridge
pull-apart
650
660
27°46'20"
27°46'00"
27°45'40"
27°45'20"
40°48'45"
0
100
200 m
6m
6m
6m
652
651
650
649
0
50 m

Figure 7

no free face was found. However, the preservation of the small-scale scarps seen in the microbathymetry requires that the sediment drape must be very thin (~10 cm?). For comparison strike-slip earthquake ruptures on land are generally associated with "mole tracks" in places where the fault rupture crosses unconsolidated sediments. Mole tracks are lines of alternating highs and lows, pressure ridges and open cracks, with small scarplets facing alternatively the two sides of the fault. For example the M 7.4 Izmit earthquake produced (as any other strike-slip earthquake of this size) a line of mole tracks with alternating topography, generally not exceeding 50 cm, while producing consistent right-lateral offsets of man-made markers reaching 5 m [*Barka et al.*, 2002]. A 10 cm thick drape of sediments would be enough to conceal most of the free faces formed along the mole tracks of the Izmit earthquake. Taking a sediment drape thickness of 10 cm and sedimentation rates ranging between 0.7–2.5 mm/yr the submarine scarp in Figure 7 would have formed 40–140 years ago. We deduce that the set of individual small-scale scarps seen with the microbathymetry and the side-scan sonar all across the Western High correspond to a very recent rupture comparable to that of the Izmit earthquake.

[27] Closer analysis of the microbathymetry in the shallowest area of the "pass" on top of the Western High reveals that the set of individual scarps has produced a consistent lateral offset of the seabottom landforms (Figure 7b). Restoring the initial geometry of these smooth landforms requires 6 ± 1 m of right-lateral slip (Figure 7c). Such a large offset may have been caused by one large event. The observed offset could also be the result of two or more successive events. If more than one earthquake have occurred, then the last one is a very recent event that has rejuvenated the morphology of the individual scarp seen in the microbathymetry by adding an incremental right-lateral slip of at least ~3 m. We conclude that a recent large earthquake with 6 m slip (or at least 3 m slip) has ruptured the entire fault segment (20 km).

3.5. Dominantly Strike-Slip Scarps in the Southeastern Tekirdag Basin: Cold Seeps, Vents, Authigenic Carbonates, Slickensides, and Evidence for the Penultimate Event

[28] The fault system at the southern edge of the Tekirdag Basin (Figures 1 and 2) has a large component of normal slip over the long term, as determined in the seismic sections [*Parke et al.*, 2002; *Okay et al.*, 2000]. So the normal faulting component appears controlling the subsidence, much like the other deep basins in Marmara (Cinarcik and Central Basins). However, the morphologic trace of this fault system can be mapped in continuity with the strike-slip fault that crosses the Western High to the east, described earlier (see Figure 2). To the west the same fault system becomes more sinuous and finally veers southwestward into a complex zone of branching with the Ganos fault, which extends farther southwestward on land. So the fault kinematics appears to vary significantly along the fault trace.

[29] Young fault scarps can be followed continuously all along the fault but they are particularly well exposed near the outlet of a submarine valley over the Tekirdag Basin floor (see Figure 2). The 3-D microbathymetry (Figure 8) reveals an outstandingly sharp, linear break at the base of a cumulative scarp about 10 m high, which may have a similar origin as the cumulative scarps described in the Central Basin. The morphologic features of the sharp break are better appreciated exactly where it crosses the valley outlet. There, the flat bottom surface appears to have been recently leveled (possibly by strong downward currents and sediment transport along the channel), producing an excellent marker for the last faulting events (see profile, Figure 8b). Thus sedimentation rates here are low, on average. The relatively uniform topography along the fault trace implies that lateral slip would not produce vertical scarps, so the vertical offsets forming both the cumulative scarp and the individual break must be associated with the component of dip slip (normal faulting) that characterizes the southern edge of the Tekirdag Basin, in addition to strike-slip.

[30] The profile in Figure 8b shows a vertical free face about 1–1.5 m high flanked by a talus slope to the north and by an eroded scarp crest to the south. Therefore the scarp associated with the last event does not explain the total vertical offset of about 2–3 m observed for the originally flat surface. This suggests that a previous event with similar throw has contributed to the total offset.

[31] The scarp with intact morphology and the free face are portrayed in the bottom imagery (Figure 9a) in the same place as described by the profile (Figure 8b). Locally the scarp appears in overhanging attitude, which suggests a secondary thrusting component. However, a close-up of the free face reveals slickensides with a rake of 15° attesting to the prevailing right-lateral motion

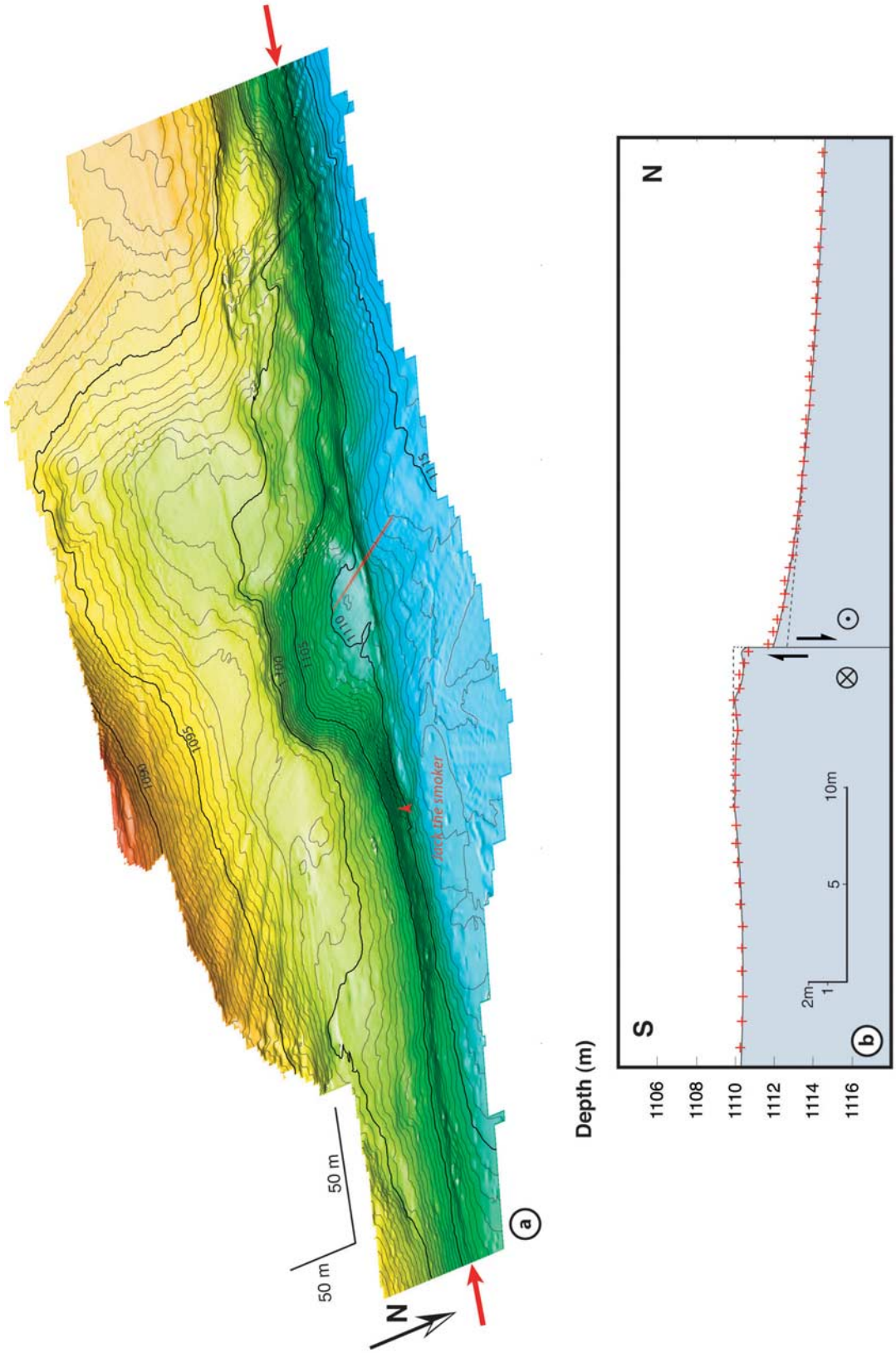
1090
1095
1100
1105
1110
1115
Dark fine smoker
50 m
50 m
N
a
S
N
Depth (m)
1106
1108
1110
1112
1114
1116
2m
1
5
10m
b

Figure 8

(Figure 9b). To be consistent with both the exposed free face and the slickensides, a net oblique slip of 4–6 m is required for the last faulting increment and about twice this amount to explain the total vertical offset of the flat surface.

[32] Conspicuous zones of cold fluid and methane seepage with associated bacterial mats, authigenic carbonate crusts and symbiotic life were discovered with the ROV in close spatial association with the submarine fault scarps, suggesting that the active fault zones control the fluid circulation within the sedimentary pile. A full description of these features is beyond the scope of this paper, but we show here a spectacular example of an active vent and associated features in the SE Tekirdag Basin, along the same set of small-scale scarps (Figure 9c; location in Figure 8).

[33] Vents and carbonate crusts appear broken and offset by the most recent scarp reactivations, offering stratigraphic evidence useful for identifying discrete events. Such a case is visible in Figure 9d, where a young flat carbonate slab appears deposited at the base of an older scarp (which is locally very well preserved), but the carbonate slab itself is ruptured parallel to the scarp by the last scarp-enlarging event, providing "field" evidence for a penultimate event which could be of similar size as the last event. Thus converging evidence (microbathymetry and "field" observations) involve the occurrence of successive earthquake ruptures of similar size on the SE Tekirdag fault. The ruptures are young, but the last one (~5 m of right-lateral slip) that is preserved with its intact tiny features must be particularly recent.

3.6. Thrust Scarps in the Southwestern Tekirdag Basin at the Ganos Fault Bend

[34] The bend where the southern Tekirdag fault system veers southwestward to meet the Ganos fault is a long-lived restraining bend (Figure 1). Since the NAF has propagated westward across the Ganos-Dardanelles region (at circa 5 Ma), a series of folds involving neogene sediments have formed successively at the Ganos bend, then transported southwestward alongside the NAF (Ganos fault) by its continuing right-lateral motion [see *Armijo et al.*, 1999, Figure 3]. A discussion of the contemporary fault geometry and kinematics, including details around the Ganos bend, is given by *Armijo et al.* [2002] (see their Figure 5).

[35] The geometry of scarps at the submarine fault bend in the southwestern Tekirdag Basin is illustrated in (Figures 10a and 10b). Fault segments about 500–800 m long and striking NE on the average are disposed in a regular right-stepping en echelon array. Here again one can check the one-to-one correspondence between scarp features seen in the microbathymetry and in the side-scan sonar images (Figures 10a and 10b). This can be made in spite of the somewhat less precise positioning of the side-scan strip. The NE-striking, right-stepping en echelon structure associated with transpression here can be compared with the NW-striking, left-stepping en echelon structure of scarps in the southern Central Basin associated with transtension (see Figures 10a, 10b, 2, 4a, and 4b). The contrast is meaningful, providing support to the inference of a component of NW-SE shortening expressed by northwestward directed thrusting as the south Tekirdag fault veers into the Ganos retraining bend.

[36] Once more small-scale individual scarps tearing a larger cumulative scarp are identified (see s1, s2 in the side-scan enlargement). In some places the en echelon structure yields multiple scarps in cross section (profile 1, Figure 10c). In other places only one fault scarp (s1) accumulates slip over the long-term (profile 2, Figure 10c).

[37] Profile 1 demonstrates that the individual scarps seen in the sonar imagery are associated with larger scarps with convex shape. That convexity is strongly suggestive of near seafloor upwarping of the leading edges of the thrust hanging walls. Those features are typical of active thrust scarps seen on land [e.g., *Bilham and Yu*, 2000]. It is interesting to compare microbathymetry profiles of en echelon scarps at the same scale, here for scarps with thrust component (profile 1 in Figure 10c) and in the Central Basin for scarps with normal fault component (Figure 4c). The stepped morphology of normal fault scarps has been replaced by rounded thrust up-warps. However, while the fine-scale features of individual

Figure 8. Morphology of combined strike- and normal-slip scarps in the southeastern Tekirdag Basin. (a) Oblique 3-D microbathymetry view of 10-m-high cumulative scarp and smaller individual break that is very linear and continuous over the sea bottom. Contours every 0.5 m. Small red crosses locate detailed profile. Red arrows indicate fault trace. (b) Enlarged profile across individual scarp with nearly vertical free face 1–1.5 m high. No vertical exaggeration. Dashed line suggests cumulative offset of initially flat bottom surface, possibly resulting from last two events. Location of active vent "Jack the smoker" is indicated.

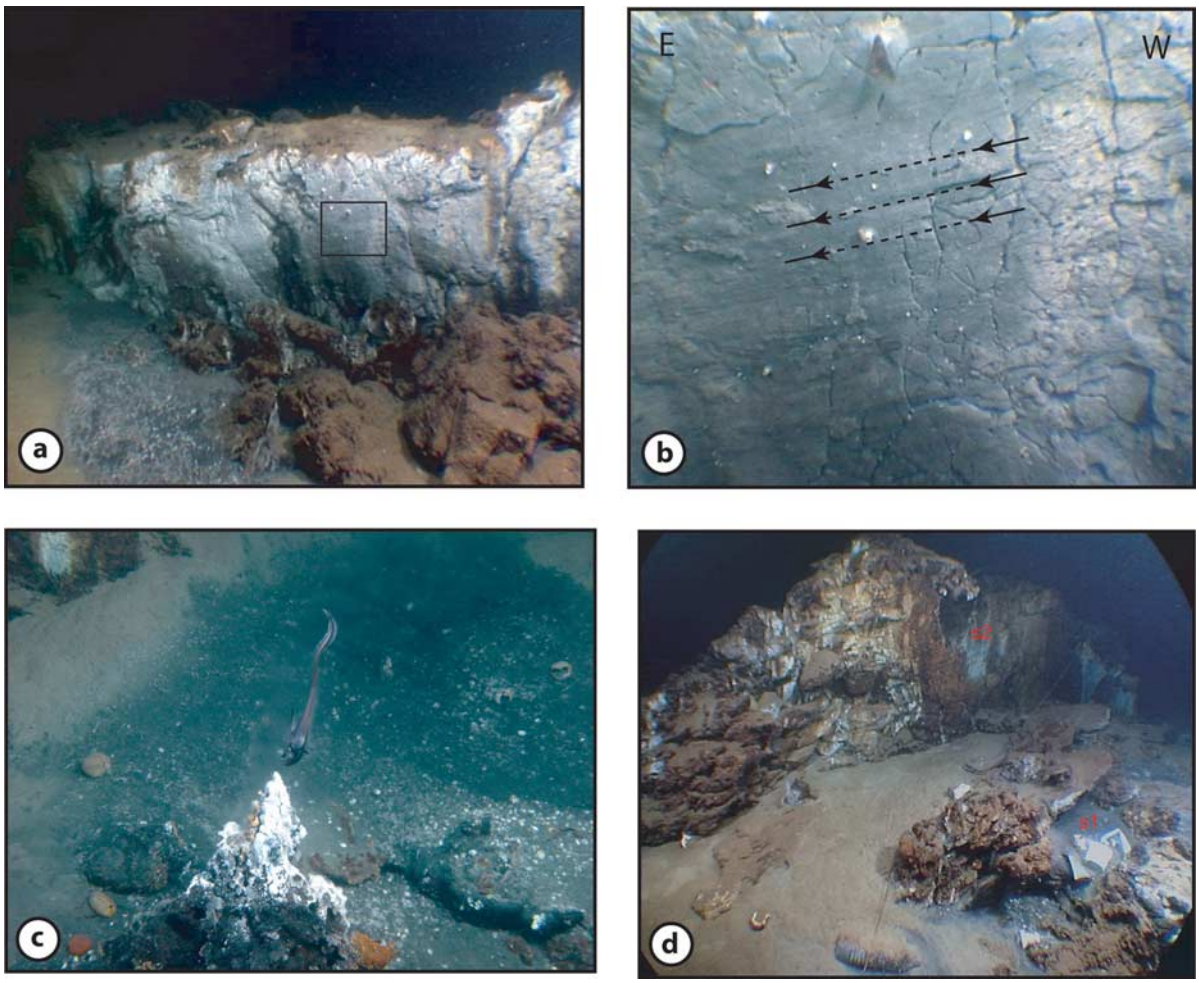

Figure 9. Sea-bottom pictures of earthquake scarps in southeastern Tekirdag Basin. (a) Fresh scarp corresponding to last event. Vertical free face 1–1.5 m high corresponds exactly to that seen in profile (Figure 8). Locally, the scarp reveals a thrusting component. The free face exposes compacted layers of white-grayish muds and sands. Black bacterial mats with small white shells and brown authigenic carbonates (broken slabs) are seen at scarp base. Carbonate-cemented sediments and bacterial mats are also present on top of the scarp. View to SE. (b) Enlargement (box in Figure 9a) shows slickensides with 15° rake substantiating dominant right-lateral motion and 4–6 m net slip for last earthquake rupture. Salient white objects are bivalve shells. View to south. (c) Cold seeps, black bacterial mats, authigenic carbonate slabs, and active vent along break. The vent (named "Jack the smoker" during the cruise, location in Figure 8) is capped by white bacterial mat. Associated chemosynthesis-dependent macrofauna includes various bivalves (abundant mytilids), echinidae, crustacea, etc. The 10-cm-long fish gives scale. View to south. (d) Horizontal authigenic carbonate slab 10 cm thick appears associated with past seepage and venting (white yogurt pot gives scale). The carbonate slab has been broken by last-earthquake rupture (right side, labeled red s1). Vertical scarp to the left (1–1.5 m high, labeled red s2) remains probably from penultimate event. View to SW.

scarps are clear in the side-scan sonar image (see enlargement), their expression in the corresponding microbathymetry profile (profile 1) is not resolved. This is possibly due to the steep local slopes at the edge of the up-warps (much like the over steepened slope for basal scarp s1 in Figure 4c). Thus within the uncertainty associated with the steep slopes we deduce a possible incremental throw of ~0.5–1 m for individual scarps s1 and s2 in profile 1. More throw is probably involved in the up-warping.

[38] Profile 2 (Figure 10c) reveals a simpler more localized structure, where a large up-warp encompasses the single cumulative scarp, near the base of which a sharp individual fault scarp (s1) has broken up to the seafloor. The large escarpment there (~10 high) appears to result from throw accumulated during several scarp-forming events; the last of them is indistinguishable from the previous ones, but it may well involve a few meters of throw.

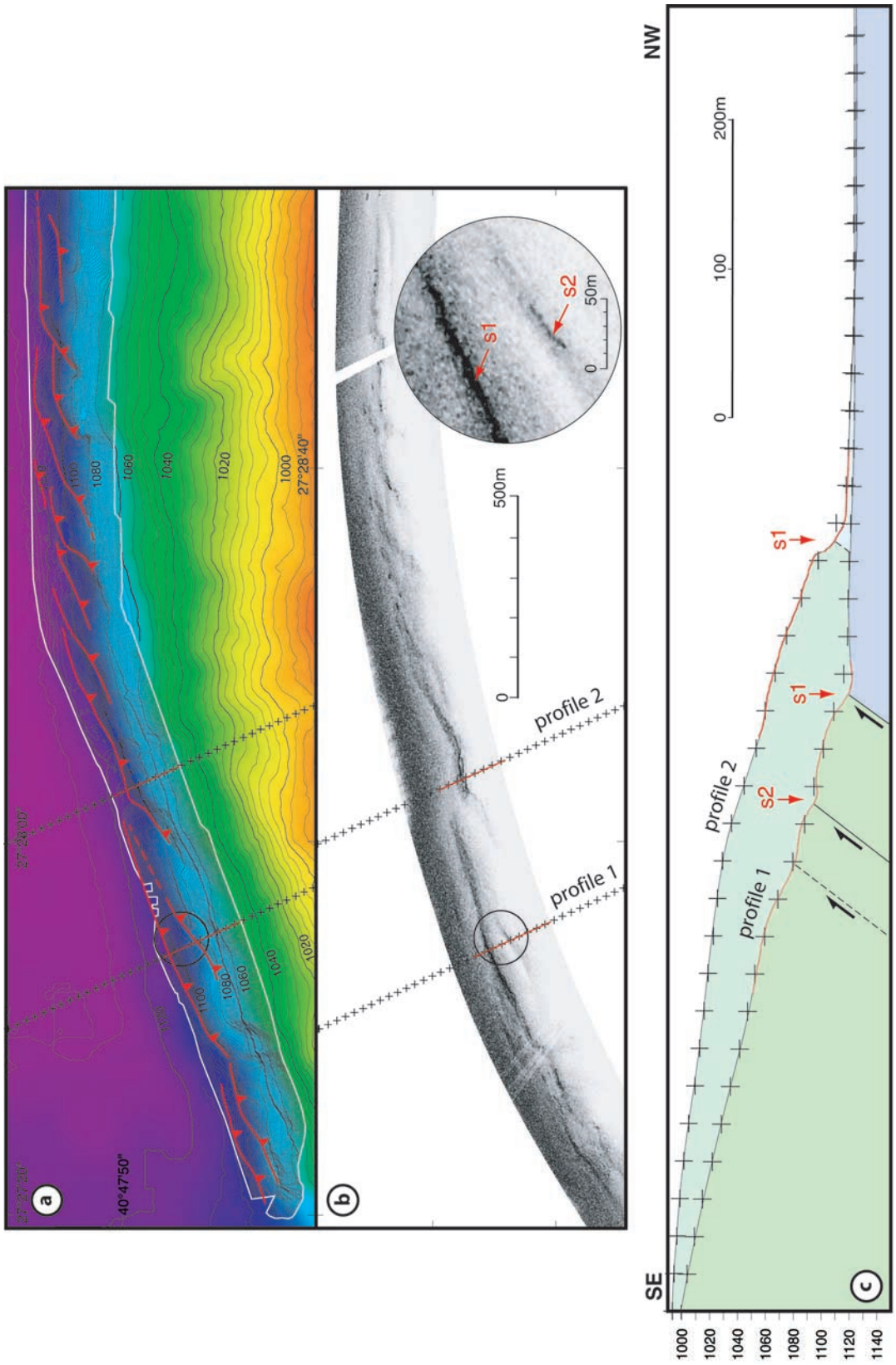
a
b
c
40°47'50"
27°27'20"
27°28'40"
1000
1020
1040
1060
1080
1100
profile 1
profile 2
s1
s2
500m
50m
0
NW
SE
200m
100
1120
1140

Figure 10

[39] Visual exploration of the area shows that the individual fault scarps are often marked by the occurrence of black bacterial mats and by small scarplets that are difficult to discriminate from the over steepened basal slopes. Exceptionally the occurrence of broken and offset authigenic carbonate slabs along the fault trace allowed us to see clear reactivation scarps about 0.5 m high. Those breaks are morphologically very similar to breaks across carbonates in the SE Tekirdag fault (see Figure 9).

[40] In summary, the configuration of the recently active scarps along the SW Tekirdag fault correlate well with the locations of the scarps seen in the side-scan sonar imagery; however, the distribution of slip during the latest event is difficult to ascertain. This difficulty seems associated with the unfavorable geometry and morphology of thrust faulting reaching the seafloor, which reveals similarly complex as thrusts reaching the surface on land. While more fragmentary, the observations of very recent scarp reactivation here are as clear as for the faults creating normal throw and comparable seafloor relief described earlier in the Central Basin. Hence the last scarp-forming earthquake may have contributed an average incremental slip comparable to that in scarps in the Central Basin (2–4 m throw with lateral slip of same order). In fact it seems very probable that the right-lateral slip associated with the last earthquake here is similar to that determined 15 km farther east along the continuation of the same fault system (~5 m).

4. Discussion

4.1. Submarine Earthquake Rupture in NW Marmara and Its Possible Age

[41] The foregoing description demonstrates that a set of youthful earthquake scarps occurs in the western part of the northern Marmara fault system. The fine-scale morphology of the submarine scarps is very well preserved. The rupture appears continuous over 60 km between the Central Basin and the Ganos bend, although it involves fault segments with different kinematics (transtension, nearly pure strike-slip and transpression). The right-lateral slip associated with the rupture is of about 5 m in the SE Tekirdag fault and possibly 6 m across the Western High. It may reach more than 2–4 m in the southern boundary fault of the Central Basin pull-apart and in the SW Tekirdag fault near the restraining Ganos bend. So, given its length and associated slip the submarine rupture must correspond to a large earthquake ($M \geq 7$). To the SW the rupture may be connected to the Ganos fault on land. To the east the rupture terminates along the southern edge of the Central Basin extensional step-over where large normal fault slip occurs (2–4 m throw). This feature is similar to the normal faulting described at the western termination of the 12 November 1999 Duzce earthquake rupture (Mw 7.2), at the southern edge of Eften lake [*Akyüz et al.*, 2002].

[42] The direct observations of submarine scarps in Marmara establish clearly that the last large scarp-forming earthquake ruptured a set of discrete segments limited to the western Sea of Marmara and that the rupture was arrested at the Central Basin step-over. There is no morphologic evidence for a continuous rupture extending further east along the whole submarine fault system. If the earthquake sequence of the 18th century ruptured as a chain of events crossing the entire Sea of Marmara, the corresponding breaks have been mostly erased or concealed.

[43] The age of the last earthquake break is difficult to assess directly with dating approaches. However, the rates of recent sedimentation of about 1–2 mm/yr determined with ^{210}Pb on shallow cores taken with the ROV near the scarps [*Schmidt et al.*, 2004] suggest that the light sediment covering the earthquake rupture (see Figures 5 and 9) could

Figure 10. Morphology of combined strike-slip and thrust scarps in the southwestern Tekirdag Basin. The submarine fault system bends from E-W to NE strike near the junction with Ganos fault (Figure 1). The fault scarps are in a clear right-stepping en echelon array. (a) Combined bathymetry (as in Figure 4). Microbathymetry has contours each 1 m. Faults in red, with triangles pointing to inferred dip direction. (b) Corresponding side-scan sonar image. Encircled close-up identifies sharp individual breaks s1 and s2 (compare with individual scarps in Figure 4b). (c) Microbathymetry profiles. Profile 1 shows that the individual scarps are at the base of larger scarps with warped morphology, suggesting shortening associated with a component of northeastward thrusting. Fault dips are unknown, but they are probably steep to accommodate the strike-slip. Dashed fault is inferred from microbathymetry only. Profile 2 shows a single cumulative scarp with convex shape. Individual scarp at its base (s1) is made of a steep escarpment about 10 m high (largely a free face) and a similar height of sediment talus. Last scarp-forming event may have contributed some meters of throw and right-lateral slip comparable to that observed farther east (Figures 8 and 9).

not be older than a century. The higher average sedimentation rates (up to 3 mm/yr) determined over the whole Holocene period with the ^{14}C dates of wood fragments in the long cores (see Figure 3) also supports this inference.

[44] From the historical seismicity in the region [*Ambraseys and Finkel*, 1995; *Ambraseys and Jackson*, 2000], the large earthquakes of 1912 or of August 1766 are the only ones that can be considered consistent with the location, the rupture length and the slip associated with the described submarine break. However, only the 1912 event is consistent with the youthful morphology and the fast sedimentation rates in Marmara. Remains of ruptures of the 18th century earthquakes would probably be less intact, less continuous and largely concealed by sediments. Regardless, there appears to be fragmentary evidence for a penultimate event of similar size in 1766 on the SE Tekirdag fault, based on the cumulative offsets recorded on the visible scarps (Figures 8b and 9d). That hypothesis seems quantitatively consistent with the pattern of intensity values assigned for the 5 August 1766 earthquake [*Parsons*, 2004]. Our observations do not provide support for the inference of seismic quiescence over the last 500 years in the northwest Sea of Marmara [*Ambraseys and Jackson*, 2000].

4.2. Previous Knowledge of the 1912 Earthquake

[45] The submarine rupture in the northwest Sea of Marmara must be compared with the relevant observations of the 1912 earthquake, which can be summarized as follows.

[46] The 9 August 1912 Ganos earthquake produced widespread damage and considerable loss of life. Surface disruptions along the Ganos fault were described in contemporary reports as ''cracks'' [*Macovei*, 1912; *Mihailovich*, 1927; *Sadi*, 1912]. No fault rupture was reported as such, but pictures of mole tracks and en echelon cracks clearly suggest prevalent right-lateral slip [*Ambraseys and Finkel*, 1987]. The significant normal slip of 3 m deduced by *Ambraseys and Finkel* [1987] appears to be mostly a secondary effect. The littoral to the southwest of where the Ganos fault enters the Sea of Marmara appears to have been slightly uplifted [*Ambraseys and Finkel*, 1987]. Such uplift is consistent with the transpressive deformation seen in submarine scarps in the southwestern Tekirdag Basin.

[47] Various authors have offered different isoseismal maps. The most recent and complete revision of macroseismic effects (estimates of local intensities reportedly within an error of ±1/2 degree of intensity) has been proposed by *Ambraseys and Finkel* [1987] and is based mainly on the precise observations by *Mihailovich* [1927]. Their two isoseismal maps can be compared in Figure 11. *Ambraseys and Finkel* [1987] deduced that coseismic faulting crossed all the land between the Gulf of Saros and Marmara with a total rupture length of 50 km. The rupture could well have extended westward some 20–30 km into the Gulf of Saros. It is worth noting that the macroseismic effects (within estimated error) suggest that the rupture may have extended several tens of kilometers under the western Sea of Marmara although without constraining precisely its termination (Figure 11).

[48] Small tsunami waves suggesting a possible submarine extension of the rupture are reported along the shores of the Sea of Marmara at the time of the 1912 event but quantification of the phenomenon appears difficult [*Mihailovich*, 1927; *Ambraseys and Finkel*, 1987, 1991]. No tide gauge record is available. Part of the difficulty comes also from the scarcity of precise reports for an event that occurred by night (main shock at 01:29 UTH; about 03:30 local time).

[49] An accurate instrumental location is not possible for the 1912 earthquake epicenter, due to the primitiveness of seismic networks. However, a reliable surface-wave magnitude Ms 7.4 ± 0.3 was calculated by *Ambraseys and Finkel* [1987] from teleseismic amplitudes from 23 Milne pendulum seismographs distributed worldwide and from amplitudes and periods from 23 mechanical instruments mainly from Europe. Hence the 1912 Ganos and the Mw 7.4 1999 Izmit earthquakes are of similar size. The 1912 earthquake was followed by numerous aftershocks of which the largest occurred a month later (Ms 6.9; 13 September 1912) [*Ambraseys and Finkel*, 1987].

[50] On the basis of field investigations carried out recently along the Ganos fault, *Altunel et al.* [2000] and *Altinok et al.* [2003] claim that some offset features associated with the 1912 event can still be identified. *Altinok et al.* [2003] deduce a maximum right-lateral slip of 4.5 m ± 0.5 m and *Altunel et al.* [2004] describe a detailed coseismic slip distribution along the Ganos fault and identify three main segments. While the poor preservation of the features may cause misidentifications

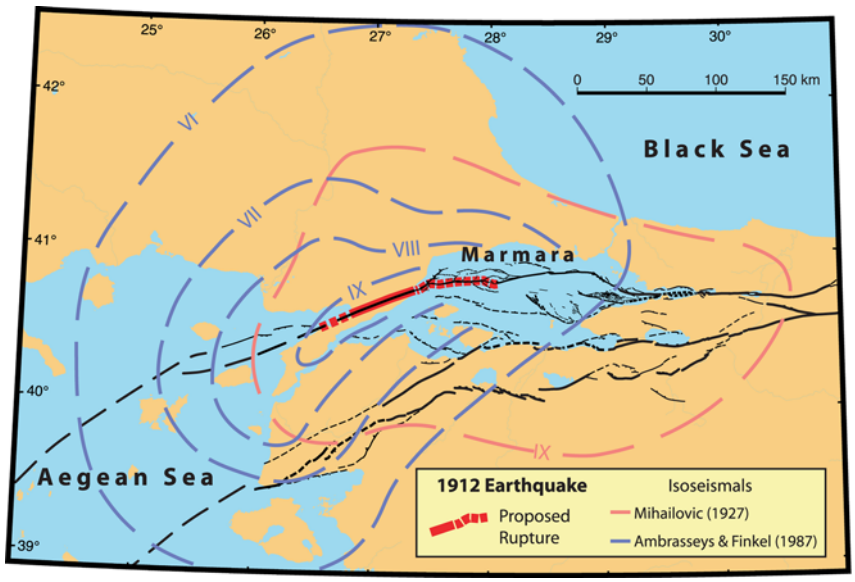

Figure 11. Possible rupture of 1912 Ganos earthquake (Ms 7.4). Proposed extent of rupture under Sea of Marmara (60 km) is consistent with observed sea-bottom break and in agreement with published isoseismals. Rupture may have reached a total length of 140 km. Isoseismals and direct observations by *Mihailovich* [1927] suggest that damage was centered in Sea of Marmara. Data revision by *Ambraseys and Finkel* [1987] suggests the rupture was restricted to the western Marmara region. Interpolations of isoseismals by *Ambraseys and Finkel* [1987] in the unpopulated Sea of Marmara have been removed.

and large uncertainties, the results appear reasonable and consistent with the contemporary descriptions by *Mihailovich* [1927]. The suggested extension of the 1912 rupture into the Sea of Marmara by *Altinok et al.* [2003] and *Altunel et al.* [2004] is similarly reasonable but nonetheless undetermined.

4.3. Assessment of the 1912 Earthquake Rupture: Implications for Present-Day Loading

[51] The submarine rupture in the northwest Sea of Marmara documented here appears much better preserved than the features attributed to the 1912 earthquake on land along the Ganos fault. Like desert conditions in continents the submarine conditions in the deep Marmara basins seem favorable to the preservation of the fine morphological features. Assuming our inference that the submarine rupture corresponds to the 1912 earthquake is correct, then the total length of the 1912 rupture is at least 110 km and possibly up to 140 km if part of the Saros Gulf has broken (Figure 11). The 1912 rupture would have crossed the restraining Ganos bend.

[52] According to GPS-based models of the regional motion the locking depth in the Northern Sea of Marmara is shallow (6–7 km) [*Meade et al.*, 2002; *Flerit et al.*, 2003; *Le Pichon et al.*, 2003]. This shallow depth is consistent with pull-apart stretching of the crust in Marmara. However, seismic activity in the North Marmara Basin extends over the upper 15 km of the crust [*Gurbuz et al.*, 2000] and the locking depth in land regions surrounding Marmara is about 18 km [*Meade et al.*, 2002; *Çakir et al.*, 2003; *Wright et al.*, 2001; *Özalaybey et al.*, 2002; *Bouchon et al.*, 2002]. So the 1912 earthquake rupture may encompass regions with contrasting locking depths, but apparently retaining everywhere significant seismic coupling. Taking average slip of 3 m over a fault plane 12 km wide and 140 km long gives a seismic moment of Mo = 1.5 10^{20} N m consistent with the instrumental surface-wave magnitude (Ms 7.4). The contribution of the submarine rupture (taking 7 km average fault width and 5 m average slip) would have been of the order of Mo = 0.6 10^{20} N m (equivalent of an earthquake with Mw 7.2), or about 40% of the total moment release.

[53] Hence the 1912 earthquake has probably relieved significant strain in NW Marmara, in spite of a possible shallow locking depth. A regional Coulomb stress distribution can be calculated for the region centered in the step-over between the

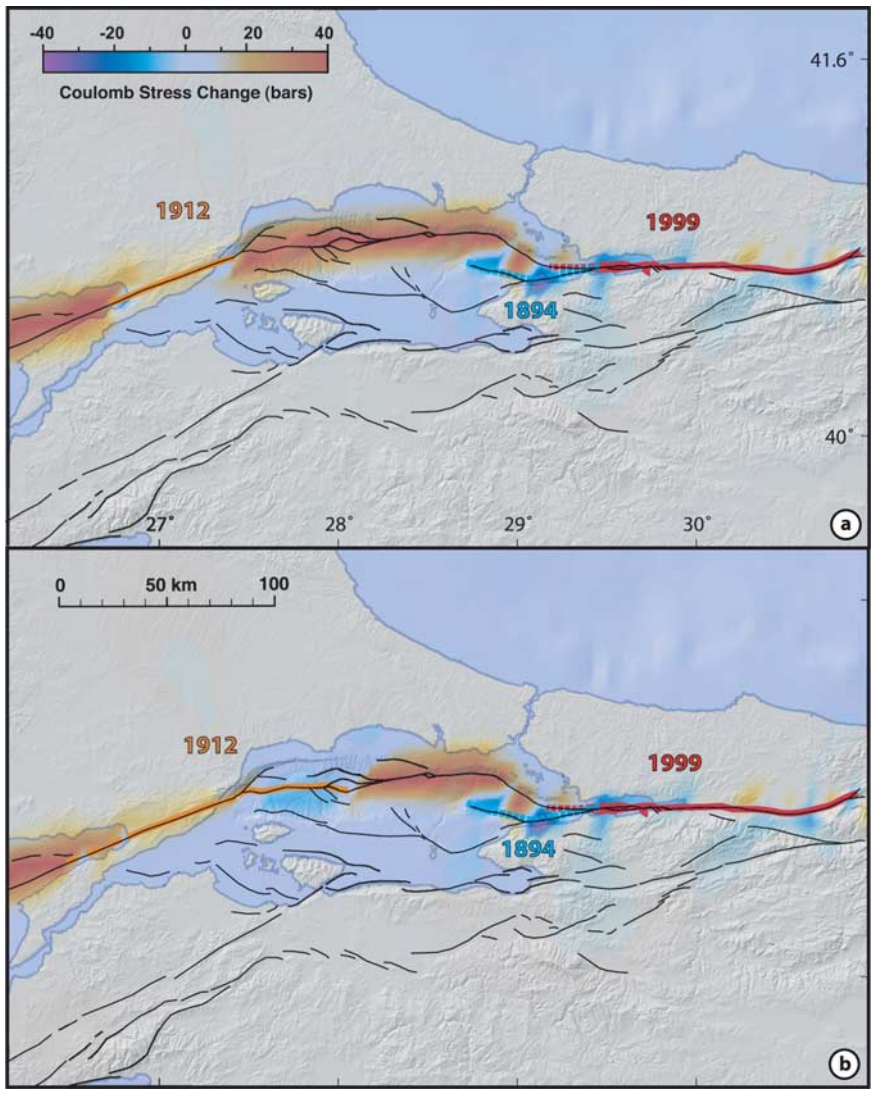

Figure 12. Coulomb modeling of stress on the North Marmara fault system. Tectonic loading is imposed since 1766 according to rates from *Flerit et al.* [2003]. Thus no assumption is made on the 18th century sequence. Since 1766 the earthquakes significantly contributing to relieve stress are the 1894 Yalova (M 7), the 1912 Ganos (Ms 7.4), and the 1999 Izmit (Mw 7.4) events. Loading and earthquakes along southern the branch of the NAF have little influence on the northern branch, so they are not represented for simplicity [*Hubert-Ferrari et al.*, 2000]. (a) Model consistent with the generally accepted idea that the 1912 earthquake rupture is limited to 50 km between Saros and Marmara [*Ambraseys and Finkel*, 1987]. The 1894 earthquake has relieved stress in Cinarkik Basin, so there the submarine fault system appears less loaded. (b) Model once the proposed 1912 submarine rupture is incorporated (total length 140 km). Elastic strain has been relieved in NW Marmara, and the zone loaded with high stresses WSW of Istanbul has significantly reduced its length.

Ganos and Izmit faults along the north branch of the NAF (Figure 12).

[54] Our modeling includes the effects of the secular tectonic loading as calculated from GPS by *Flerit et al.* [2003]. Secular loading deduced by *Meade et al.* [2002] and *Le Pichon et al.* [2003] is kinematically inappropriate for this purpose as discussed earlier. For simplicity no hypothesis is made concerning the possible zones of rupture associated with the large earthquakes of the 18th century and so the secular tectonic loading is imposed only after the end of the sequence (since 1766). After that, the calculations of contemporary Coulomb stress for the step-over depend critically on the stress relieve associated with the subsequent three major earthquakes, which are the 1894 Yalova (M 7), the 1912 Ganos (Ms 7.4) and the

1999 Izmit (Mw 7.4) earthquakes. Including the smaller 1963 Cinarcik (Ms 6.4) earthquake in our calculations does not change significantly the first-order picture we discuss here.

[55] For the 1999 earthquake we take slip consistent with results from the SAR interferometry as discussed by *Çakir et al.* [2003], which provide good constraints for slip in the Izmit Gulf. For the 1894 earthquake we impose a rupture on the SW Cinarcik fault consistent with intensity observations discussed by *Parsons* [2004] and with our ROV observations. Then a model for the generally accepted hypothesis that the 1912 Ganos earthquake rupture did not enter far into Marmara [*Ambraseys and Finkel*, 1987, 1991; *Hubert-Ferrari et al.*, 2000; *Ambraseys and Jackson*, 2000] can be compared with a model incorporating the 60-km-long submarine part of the rupture in NW Marmara as discussed earlier (Figure 12).

[56] The consequences of this change are important. The 1912 earthquake in NW Marmara is assumed to leave that region with stress build-up only since then, which corresponds to a little less than 2 m of slip of the fault system at depth, at the secular rate of 20 mm/yr [*Flerit et al.*, 2003]. So the slip deficit in the NW Marmara region is now the same as the deficit in the Ganos fault on land, despite possible differing rupture histories prior to 1912. However, the submarine rupture of 1912 can be seen as discharging strain accumulated there for at least 146 years, since the 5 August 1766 event.

[57] The eastern region between the Central Basin and the 1999 Izmit rupture is about 100 km long, including two joining fault segments with distinctively different strike and kinematics, which make a clear angle south of Istanbul (see Figures 1 and 2). The NW-striking segment at the base of the large escarpment to the NE of the Cinarcik Basin has a significant component of normal slip whereas the linear EW-striking segment connecting the Cinarcik Basin with the Central Basin has nearly pure strike-slip [*Armijo et al.*, 2002]. Another fault segment with normal slip is to the SW of the Cinarcik Basin. Thus three segments could break during separate large earthquakes in the east Marmara region, where strain is probably accumulating since the 18th century sequence (1754 and 22 May 1766 events), possibly with significant discharge in 1894 (M$\sim$7) and minor release in 1963 (Ms 6.4) [*Ambraseys and Jackson*, 2000; *Parsons*, 2004]. By incorporating discharge due to the 1894 earthquake Coulomb stress has been reduced for faults in the Cinarcik Basin. The slip deficit accumulated since 1894 would probably not exceed 2 m in Cinarcik. Thus only the 70-km-long strike-slip segment between the Cinarcik and Central Basins would be substantially loaded, corresponding to 4–5 m of slip deficit, or more if this segment had not ruptured since 1509 [*Ambraseys and Jackson*, 2000].

[58] Taking again a narrow fault width of 7 km and the deduced slip deficits of 4–5 m and 2 m (for the strike-slip central Marmara and the transtensional Cinarcik segments) a total potential for a Mo = 0.8 10^{20} N m (Mw 7.2–7.3) earthquake can be deduced for the overall east Marmara region. The separate contribution of a rupture with a component of normal faulting in the Cinarcik Basin could be as much as Mo = 0.2 10^{20} N m (or about Mw 6.8). The contribution of a strike-slip rupture of the segment between the Cinarcik and Central Basins would be Mo = 0.7 10^{20} N m (Mw 7.2). Other combinations involving smaller subsegments are possible. An example is the Ms 6.4 1963 earthquake, which probably has ruptured part of the NE Cinarcik fault (Figures 1 and 2). A maximized fault width of 10 km would increase to Mw 7.3–7.4 the maximum magnitude of an earthquake rupturing the overall east Marmara region.

[59] The hypothesis of a future large-magnitude earthquake (Mw 7.6–7.7) with a 175-km-long throughgoing rupture across Marmara has been put forward insistently in recent years [*Le Pichon et al.*, 1999, 2003; *Sengör et al.*, 2004]. Nothing in the scarp evidence described here or in the historical seismicity analyzed by *Ambraseys and Finkel* [1991], *Ambraseys and Jackson* [2000], and *Parsons* [2004] appears to support a past rupture of that nature. The possible slip deficits and the Coulomb stress modeling do not favor full rupture of the segmented fault system during a future event either. While it is impossible to rule-out such event, it appears less probable than the alternatives discussed earlier.

5. Conclusions

[60] The new geomorphologic and geologic evidence allows an accurate description of active submarine faults in the Sea of Marmara, next to Istanbul. Those faults exhibit earthquake scarps associated with recent historic events. The quality and dense coverage of observations using complementary high-resolution sensors (bathymetry and shallow penetration profiling), sediment cores and ^{14}C ages are comparable to the best standards in

studies of active faults on land. Some major conclusions are:

[61] 1. The ^{14}C-calibrated ages constrain the evolution of the morphology and the shallow subbottom stratigraphy during the last Glacial-Interglacial transition including a sharp change after ~14 ka from lake to marine conditions in Marmara. The submarine scarps in the northern Sea of Marmara floor have formed by accumulation of earthquake slip under competing tectonic, erosion and sedimentation processes subject to climatic change. The visible fault scarps in the seafloor have emerged progressively after the occurrence of catastrophic sedimentary events associated with deglaciation.

[62] 2. Sedimentation rates in the deep pull-apart basins are fast (1–3 mm/yr), but they do not keep up with even faster fault rates and associated subsidence that create the deep bathymetric sinks. The normal faulting throw rates are up to 6 mm/yr at pull-apart margins. Throw and right-lateral slip rates deduced from the scarp evidence are consistent with rates deduced at larger scale from geology and GPS.

[63] 3. The geometry of submarine scarps in Marmara requires a combination of strike-slip and normal faulting consistent with the segmentation of the pull-apart fault system defined with bathymetry [*Armijo et al.*, 2002] and multichannel seismics [*Hirn et al.*, 2003]. Accordingly earthquake scarps have formed mostly under transtension and strike-slip conditions, but transpression scarps have formed at the restraining Ganos bend.

[64] 4. The submarine earthquake scarps found in Marmara are in very good state of preservation in spite of the fast sedimentation rates. The last earthquake scarps rupturing the north Marmara fault system are discrete events, not breaking continuously the large extensional step-over between the Ganos fault and the Izmit fault. So the direct observations of submarine scarps in Marmara help defining the barriers that have arrested past earthquake ruptures as well as defining the possible segmentation of the contemporary state of loading.

[65] 5. Stunning youthful earthquake scarps extend offshore from these two faults into the Sea of Marmara. One enters a modest distance into the Cinarcik Basin and is readily attributed to the eastward extension of the 17 August 1999 Izmit (Mw 7.4) earthquake [*Çakir et al.*, 2003]. The other cuts a significant length in the Tekirdag Basin, the Western High and the Central Basin. It is the key discovery discussed in this paper.

[66] 6. Two other fault breaks are apparent at the normal fault edges of the Cinarcik Basin. A small fresh break 20–30 km long is identified in the NE Cinarcik Basin fault and correlated tentatively with the 18 October 1963 (Ms 6.4) earthquake. The large fault (50 km long) recognized at the southern edge of the Cinarkik Basin has at its base scarps with over-steepened slopes suggesting it may have ruptured during the 10 July 1894 (M~7) earthquake.

[67] 7. The submarine earthquake rupture in NW Marmara is exceptionally well preserved over 60 km. Studying its fine-scale morphology allows us to determine a right-lateral slip of 5 m associated with the last scarp-forming event. Normal throw of up to 2–4 m characterizes the eastern end of the rupture in the Central Basin extensional step-over, which thus appears to have arrested the rupture. The fast sedimentation rates in the deep Marmara basins strongly suggest that this youthful rupture is associated with the 9 August 1912 (Ms 7.4) earthquake. Evidence for a more concealed scarp associated with a large penultimate event in the same submarine region could correspond to rupture of the 5 August 1766 (M~7.4) earthquake.

[68] 8. Thus the Ms 7.4 1912 Ganos earthquake has probably ruptured fault segments on the two sides of the Ganos restraining bend, from the Gulf of Saros to the Central Basin in Marmara, over a total length of about 140 km, not 50 km as previously thought [*Ambraseys and Finkel*, 1987]. The scarp evidence is consistent with macroseismic observations and published isoseismals [*Mihailovich*, 1927; *Ambraseys and Finkel*, 1987]. Unsurprisingly the Ms 7.4 Ganos earthquake appears to have similar rupture length as the Mw 7.4 Izmit earthquake. The consequences when estimating the contemporary state of loading in the region are very important.

[69] 9. Coulomb stress modeling incorporating the new submarine scarp evidence shows that the discharge associated with the 1912 rupture may have significantly reduced the length of the zone with high stresses in NW Marmara, while the 1894 rupture has probably reduced stresses in the eastern Cinarcik Basin. Maximum contemporary loading with at least 4–5 m of slip deficit would occur at the strike-slip segment 70 km long between the Cinarcik and Central Basins, which may have not ruptured since the 18th century earthquake se-

quence. The probable rupture of that segment alone would represent a seismic moment of Mo = 7 10^{19} N m (Mw = 7.2). Adding simultaneous rupture of the Cinarcik segment would give a total moment of Mo = 0.8 10^{20} N m (Mw = 7.2–7.3) for the overall east Marmara region. Scenarios with events involving separate segments are plausible. Maximized events with much longer rupture across the Sea of Marmara appear less probable.

Acknowledgments

[70] We wish to dedicate this work to the memory of our friend Aykut Barka, who was always present in our minds during the course of this extraordinary adventure. The MARMARASCARPS cruise was performed within the framework of the collaborative program on the seismic risk in the Istanbul and Sea of Marmara region coordinated by the Turkish TUBITAK and the French INSU-CNRS, with support from the French Ministry of Foreign Affairs (MAE). Crucial for this cruise was the enthusiastic and always very positive help provided by Philippe Vidal from INSU. Yves Gallet is also acknowledged for affirmative help to the program. Naci Görür from TUBITAK must be thanked for coordinating the effort in Turkey. Rear Admiral of the Turkish Navy Nazim Çubukçu from SHOD has kindly provided all the necessary support for navigating safely in the Sea of Marmara. S. Nahirci and E. Hacioglu contributed to that purpose aboard Atalante. We wish to thank warmly captain Alix and all the crew of Atalante, as well as the team of pilots of the ROV Victor 6000, led efficiently by A. Christophe. The IFREMER was specifically associated in this venture for this first very extensive survey using experimentally the multibeam microbathymetry facility mounted on the ROV Victor 6000. Vincent Rigaud from DNIS/IFREMER has taken the responsibility of this technical issue. Very special thanks go to the team led by Jan Opderbecke, who successfully installed and courageously operated the microbathymetry facility on board: Anne-Gaëlle Vincent, Henri Martinossi, and Toussaint Edmond. Geoff King and Steve Wesnousky are acknowledged for stimulating constructive comments. Jordan Muller and an anonymous reviewer made thorough reviews. Celal Sengör is also thanked. This is Institut de Physique du Globe de Paris (IPGP) paper 2044. INSU paper 380.

References

Akyüz, H. S., R. Hartleb, A. Barka, E. Altunel, G. Sunal, B. Meyer, and R. Armijo (2002), Surface rupture and slip distribution of the 12 November 1999 Düzce earthquake (M 7.1), north Anatolian Fault, Bolu, Turkey, *Bull. Seism. Soc. Am*, *92*, 61–66.

Altinok, Y., B. Alpar, and C. Yaltirak (2003), Sarköy-Mürefte 1912 earthquake's tsunami: Extension of the associated faulting in the Marmara Sea, Turkey, *J. Seismol.*, *7*, 329–346.

Altunel, E., A. Barka, and S. Akyüz (2000), Slip distribution along the 1912 Mürefte-Sarköy earthquake, North Anatolian Fault, western Marmara, in *The 1999 Izmit and Duzce Earthquakes: Preliminary Results*, edited by A. Barka et al., pp. 341–349, Istanbul Tech. Univ., Istanbul, Turkey.

Altunel, E., M. Meghraoui, H. S. Akyüz, and A. Dikbas (2004), Characteristics of the 1912 co-seismic rupture along the North Anatolian Fault Zone (Turkey): Implications for the expected Marmara earthquake, *Terra Nova*, *16*, doi:10.1111/j.1365-3121.2004.00552.x, 198–204.

Ambraseys, N. (1988), Engineering seismology, *Earthquake Eng. Struct. Dyn.*, *17*, 1–105.

Ambraseys, N., and C. Finkel (1987), The Saros-Marmara earthquake of 9 August 1912, *Earthquake Eng. Struct. Dyn.*, *15*, 189–211.

Ambraseys, N. N., and C. Finkel (1991), Long-term seismicity of Istanbul and of the Marmara Sea region, *Terra Nova*, *3*, 527–539.

Ambraseys, N., and C. Finkel (1995), *The Seismicity of Turkey and Adjacent Areas 1500–1800*, 240 pp., Eren Yayincilik ve Kitapcilik, Istanbul, Turkey.

Ambraseys, N. N., and J. A. Jackson (2000), Seismicity of the Sea of Marmara (Turkey) since 1500, *Geophys. J. Int.*, *141*, F1–F6.

Armijo, R., P. Tapponnier, J. L. Mercier, and H. Tonglin (1986), Quaternary extension in southern Tibet: Field observations and tectonic implications, *J. Geophys. Res.*, *91*, 13,803–13,872.

Armijo, R., P. Tapponnier, and H. Tonglin (1989), Late Cenozoic right-lateral strike-slip faulting in southern Tibet, *J. Geophys. Res.*, *94*, 2787–2938.

Armijo, R., H. Lyon-Caen, and D. Papanastassiou (1991), A possible normal-fault rupture for the 464 B.C. Sparta earthquake, *Nature*, *351*, 137–139.

Armijo, R., H. Lyon-Caen, and D. Papanastassiou (1992), E-W extension and Holocene normal fault scarps in the Hellenic Arc, *Geology*, *20*, 491–494.

Armijo, R., B. Meyer, A. Hubert, and A. Barka (1999), Westward propagation of the North Anatolian fault into the northern Aegean: Timing and kinematics, *Geology*, *27*(3), 267–270.

Armijo, R., B. Meyer, A. Hubert, and A. Barka (2000), Westward propagation of the North Anatolian fault into the northern Aegean: Timing and kinematics: Reply, *Geology*, *28*(2), 188–189.

Armijo, R., B. Meyer, S. Navarro, G. King, and A. Barka (2002), Asymmetric slip partitioning in the Sea of Marmara pull-apart: A clue to propagation processes of the North Anatolian Fault, *Terra Nova*, *14*(2), 80–86.

Armijo, R., F. Flerit, G. King, and B. Meyer (2003), Linear elastic fracture mechanics explains the past and present evolution of the Aegean, *Earth Planet. Sci. Lett.*, *217*, 85–95.

Avouac, J. P., P. Tapponnier, M. Bai, H. You, and G. Wang (1993), Active thrusting and folding along the northern Tien Shan and late Cenozoic rotation of the Tarim relative to Dzungaria and Kazakhstan, *98*(B4), 6755–6804.

Barka, A., and K. Kadinsky-Cade (1988), Strike-slip fault geometry in Turkey and its influence on earthquake activity, *Tectonics*, *7*, 663–684.

Barka, A., et al. (2002), The surface rupture and slip distribution of the 17 August 1999 Izmit earthquake M 7.4, North Anatolian fault, *Bull. Seismol. Soc. Am.*, *92*, 43–60.

Beck, C., et al. (2003), Late Pleistocene major sedimentary reworking event (homogenite) in the Marmara Sea Central Basin: A combination of Late Glacial high terrigenous supply with a major earthquake? Preliminary results of giant piston-coring and high-resolution seismic reflexion, *Geophys. Res. Abstr.*, *5*, abstract 13126.

Benedetti, L., R. Finkel, D. Papanastassiou, G. King, R. Armijo, F. Ryerson, D. Farber, and F. Flerit (2002), Post-glacial slip history of the Sparta fault (Greece) determined by ^{36}Cl cosmogenic dating: Evidence for non-periodic earthquakes, *Geophys. Res. Lett.*, *29*(8), 1246, doi:10.1029/2001GL014510.

Benedetti, L., R. Finkel, G. King, R. Armijo, D. Papanastassiou, F. Ryerson, F. Flerit, D. Farber, and G. Stavrakakis (2003), Motion on the Kaparelli fault (Greece) prior to the 1981 earthquake sequence determined from ^{36}Cl cosmogenic dating, *Terra Nova*, *15*, 118–124.

Bilham, R., and T.-T. Yu (2000), The morphology of thrust faulting in the 21 September 1999, Chichi, Taiwan earthquake, *J. Asian Earth Sci.*, *18*, 351–367.

Bouchon, M., M. N. Töksoz, H. Karabulut, M. P. Bouin, M. Dietrich, M. Aktar, and M. Edie (2002), Space and time evolution of rupture and faulting during the 1999 the Izmit (Turkey) earthquake, *Bull. Seismol. Soc. Am.*, *92*(1), 256–266.

Çagatay, N., N. Görür, A. Algan, C. Eastoe, A. Tchapalyga, D. Ongan, T. Kuhn, and I. Kuscu (2000), Late Glacial-Holocene palaeoceanography of the Sea of Marmara: Timing of connections with the Mediterranean and the Black Seas, *Mar. Geol.*, *167*, 191–206.

Çagatay, N., N. Görür, A. Polonia, E. Demirbag, M. Sakinç, M.-H. Cormier, L. Capotondi, C. McHugh, O. Emre, and K. Eris (2003), Sea-level changes and depositional environments in the Izmit Gulf, eastern Marmara Sea, during the late glacial-Holocene period, *Mar. Geol.*, *202*, 159–173.

Çakir, Z., J.-B. de Chabalier, R. Armijo, B. Meyer, A. Barka, and G. Peltzer (2003), Coseismic and early postseismic slip associated with the 1999 Izmit earthquake (Turkey), from SAR interferometry and tectonic field observations, *Geophys. J. Int.*, *155*, 93–110.

Carton, H. (2003), Structure of the Cinarcik Basin (eastern Marmara Sea) from densely-spaced multi-channel reflection profiles, Lithos Science Report, pp. 69–76, Bullard Lab., Univ. of Cambridge, Cambridge, UK.

Demirbag, E., C. Rangin, X. Le Pichon, and A. M. C. Sengor (2003), Investigation of the tectonics of the Main Marmara Fault by means of deep-towed seismic data, *Tectonophysics*, *361*, 1–19.

Feigl, K. L., F. Sarti, H. Vadon, S. McClusky, S. Ergintav, P. Durand, R. Bürgmann, A. Rigo, D. Massonnet, and R. Reilinger (2002), Estimating slip distribution for the Izmit mainshock from coseismic GPS, ERS-1, RADARSAT, and SPOT measurements, *Bull. Seismol. Soc. Am.*, *92*, 138–160.

Flerit, F., R. Armijo, G. C. P. King, B. Meyer, and A. Barka (2003), Slip partitioning in the Sea of Marmara Pull-Apart determined from GPS velocity vectors, *Geophys. J. Int.*, *154*, 1–7.

Flerit, F., R. Armijo, G. King, and B. Meyer (2004), The mechanical interaction between the propagating North Anatolian Fault and the back-arc extension in the Aegean, *Earth Planet. Sci. Lett.*, *224*, 347–362.

Gurbuz, C., et al. (2000), The seismotectonics of the Marmara region (Turkey): Results from a microseismic experiment, *Tectonophysics*, *316*, 1–17.

Hanks, T. C., R. C. Bucknam, K. R. Lajoie, and R. E. Wallace (1984), Modification of wave-cut and faulting-controlled landforms, *J. Geophys. Res.*, *89*, 5771–5790.

Hirn, A., et al. (2003), Elements of structure at crustal scale under the Sea of Marmara from multichannel seismics of the SEISMARMARA survey, *Geophys. Res. Abstr.*, *5*, abstract 13126.

Hubert-Ferrari, A., A. Barka, E. Jacques, S. Nalbant, B. Meyer, R. Armijo, P. Tapponnier, and G. C. P. King (2000), Seismic hazard in the Marmara Sea following the 17 August 1999 Izmit earthquake, *Nature*, *404*, 269–272.

Hubert-Ferrari, A., R. Armijo, G. King, B. Meyer, and A. Barka (2002), Morphology, displacement, and slip rates along the North Anatolian Fault, Turkey, *J. Geophys. Res.*, *107*(B10), 2235, doi:10.1029/2001JB000393.

Imren, C., X. Le Pichon, C. Rangin, E. Demirbag, B. Ecevitoglu, and N. Görür (2001), The North Anatolian fault within the Sea of Marmara: A new evaluation based on multichannel seismic and multibeam data, *Earth Planet. Sci. Lett.*, *186*, 143–158.

Karabulut, H., M. P. Bouin, M. Bouchon, M. Dietrich, C. Cornou, and M. Aktar (2002), The seismicity in the eastern Marmara Sea after the 17 August 1999 Izmit earthquake, *Bull. Seismol. Soc. Am.*, *92*, 387–393.

Le Pichon, X., T. Taymaz, and A. M. C. Sengor (1999), The Marmara Fault and the future Istanbul earthquake, in *International Conference on the Kocaeli Earthquake, 17 August 1999*, edited by M. Karaça and D. N. Ural, pp. 41–54, Istanbul Tech. Univ. Press House, Istanbul, Turkey.

Le Pichon, X., T. Taymaz, and A. M. C. Sengor (2000), Important problems to be solved in the Sea of Marmara (abstract), in *NATO Advanced Research Seminar: Integration of Earth Sciences Research on the 1999 Turkish and Greek Earthquakes and Needs for Future Cooperative Research*, edited by N. Görür, pp. 66–67, TÜBITAK, Istanbul, Turkey.

Le Pichon, X., et al. (2001), The active main Marmara fault, *Earth Planet. Sci. Lett.*, *192*, 595–616.

Le Pichon, X., N. Chamot-Rooke, C. Rangin, and A. M. C. Sengör (2003), The North Anatolian fault in the Sea of Marmara, *J. Geophys. Res.*, *108*(B4), 2179, doi:10.1029/2002JB001862.

Macovei, R. (1912), Sur le tremblement de terre de la Mer de Marmara le 9 Août 1912, *Bull. Sect. Sci. Acad. Roumaine*, *1*, 1–9.

McClusky, S., et al. (2000), Global Positioning System constraints on the plate kinematics and dynamics in the eastern Mediterranean and Caucasus, *J. Geophys. Res.*, *105*, 5695–5719.

McNeill, L. C., A. Mille, T. A. Minshull, J. M. Bull, N. H. Kenyon, and M. Ivanov (2004), Extension of the North Anatolian Fault into the North Aegean Trough: Evidence for transtension, strain partitioning, and analogues for Sea of Marmara basin models, *Tectonics*, *23*, TC2016, doi:10.1029/2002TC001490.

Meade, B. J., B. H. Hager, S. McClusky, R. Reilinger, S. Ergintav, O. Lenk, A. Barka, and H. Ozener (2002), Estimates of seismic potential in the Marmara Sea region from block models of secular deformation constrained by Global Positioning System measurements, *Bull. Seismol. Soc. Am.*, *92*, 208–215.

Mercier de Lépinay, B., et al. (2003), Interplay between recent sedimentation and active tectonics in Marmara Sea, *Geophys. Res. Abstr.*, *5*, abstract 13126.

Mériaux, A.-S., F. J. Ryerson, P. Tapponnier, J. Van der Woerd, R. C. Finkel, X. Xu, Z. Xu, and M. W. Caffee (2004), Rapid slip along the central Altyn Tagh Fault: Morphochronologic evidence from Cherchen He and Sulamu Tagh, *J. Geophys. Res.*, *109*, B06401, doi:10.1029/2003JB002558.

Meyer, B., P. Tapponnier, L. Bourjot, F. Métivier, Y. Gaudemer, G. Peltzer, G. Shunmin, and C. Zitai (1998), Crustal thickening in Gansu-Qinghai, lithospheric mantle subduction, and oblique, strike slip controlled growth of the Tibet Plateau, *Geophys. J. Int.*, *135*, 1–47.

Mihailovich, J. (1927), Trusne katastrofe na Mramornome moru, *Posebno Izdan*, *65*(16), 303 pp.

Muller, J. R., and A. Aydin (2005), Using mechanical modeling to constrain fault geometries proposed for the northern Marmara Sea, *J. Geophys. Res.*, *110*, B03407, doi:10.1029/2004JB003226.

Nalbant, S. S., A. Hubert, and G. C. P. King (1998), Stress coupling between earthquakes in northwest Turkey and the North Aegean Sea, *J. Geophys. Res.*, *103*, 24,469–24,486.

Okay, A., E. Demirbag, H. Kurt, N. Okay, and I. Kuscu (1999), An active, deep marine strike-slip basin along the North Anatolian fault in Turkey, *Tectonics*, *18*(1), 129–147.

Okay, A. I., A. Kaslilar-Ozcan, C. Imren, A. Boztepe-Guney, E. Demirbag, and I. Kuscu (2000), Active faults and evolving strike-slip fault basins in the Marmara Sea, northwest Turkey: A multichannel reflection study, *Tectonophysics*, *312*, 189–218.

Özalaybey, S., M. Ergin, M. Aktar, C. Tapirdamaz, F. Biçmen, and A. Yörük (2002), The 1999 Izmit earthquake sequence in Turkey: Seismological and tectonic aspects, *Bull. Seismol. Soc. Am.*, *92*(1), 376–386.

Parke, J. R., R. S. White, D. McKenzie, T. A. Minshull, J. M. Bull, I. Kuşçu, N. Görür, and C. Şengör (2002), Interaction between faulting and sedimentation in the Sea of Marmara, western Turkey, *J. Geophys. Res.*, *107*(B11), 2286, doi:10.1029/2001JB000450.

Parsons, T. (2004), Recalculated probability of $M \geq 7$ earthquakes beneath the Sea of Marmara, Turkey, *J. Geophys. Res.*, *109*, B05304, doi:10.1029/2003JB002667.

Parsons, T., S. Toda, R. S. Stein, A. Barka, and J. H. Dieterich (2000), Heightened odds of large earthquakes near Istanbul: An interaction-based probability calculation, *Science*, *288*, 661–665.

Peltzer, G., P. Tapponnier, Y. Gaudemer, B. Meyer, S. Guo, S. Yin, Z. Chen, and H. Dai (1988), Offsets of late Quaternary morphology, and recurrence of large earthquakes on the Chang Ma fault (Gansu, China), *J. Geophys. Res.*, *93*, 7793–7812.

Polonia, A., et al. (2004), Holocene slip rate of the North Anatolian Fault beneath the Sea of Marmara, *Earth Planet. Sci. Lett.*, *227*, 411–426.

Rangin, C., X. Le Pichon, E. Demirbag, and C. Imren (2004), Strain localization in the Sea of Marmara: Propagation of the North Anatolian Fault in a now inactive pull-apart, *Tectonics*, *23*, TC2014, doi:10.1029/2002TC001437.

Reilinger, R. E., et al. (2000), Coseismic and postseismic fault slip for the 17 August 1999 M = 7.5, Izmit, Turkey earthquake, *Science*, *289*, 1519–1524.

Ritz, J.-F., et al. (2003), Late Pleistocene to Holocene slip rates for the Gurvan Bulag thrust fault (Gobi-Altay, Mongolia) estimated with ^{10}Be dates, *J. Geophys. Res.*, *108*(B3), 2162, doi:10.1029/2001JB000553.

Rockwell, T., A. Barka, T. Dawson, H. S. Akyüz, and K. Thorup (2001), Paleoseismology of the Gaziköy-Saros segment of the North Anatolian fault, northwestern Turkey: Implications of regional seismic hazard and models of earthquake recurrence, *J. Seismology*, *5*, 433–448.

Sadi, M. (1912), Marmara Havzasýnýn 26–27 Temmuz Hareket-i Arzi 15 Eylul 1328, Resimli Kitap Mat, *Bull. Am. Astron. Soc.*, *1*, 45 pp.

Schindler, C. (1998), Geology of NW Turkey: Results of the Marmara polyproject, in *Active Tectonics of Northwestern Anatolia: The Marmara Poly-Project, a Multidisciplinary Approach by Space-Geodesy, Geology, Hydrology, Geothermics and Seismology*, edited by C. Schindler and M. Pfister, pp. 329–375, Verlag der Fachvereine, Zurich, Switzerland.

Schmidt, S., O. Weber, J.-M. Jouanneau, R. Armijo, I. Lefevre, C. Beck, and N. Pondard (2004), Tentative de datation des séismes récents en Mer de Marmara par l'utilisation combinée de l'imagerie X et du ^{210}Pb, paper presented at Congrès ASF, Assoc. des Sédiment. Fr., Bordeaux, France, 11–19 Oct.

Seeber, L., O. Emre, M.-H. Cormier, C. C. Sorlien, C. McHugh, A. Polonia, N. Ozer, and N. Çagatay (2004), Uplift and subsidence from oblique slip: The Ganos-Marmara bend of the North Anatolian Transform, western Turkey, *Tectonophysics*, *391*, 239–258.

Sengör, A. M. C., O. Tüysüz, C. Imren, M. Sakinç, H. Eyidogan, N. Görür, X. Le Pichon, and C. Rangin (2004), The North Anatolian Fault: A new look, *Annu. Rev. Earth Planet. Sci.*, *33*, 1–75.

Stein, R. S., A. A. Barka, and J. H. Dieterich (1997), Progressive failure on the North Anatolian fault since 1939 by earthquake stress triggering, *Geophys. J. Int.*, *128*, 594–604.

Straub, C., H.-G. Kahle, and C. Schindler (1997), GPS and geologic estimates of the tectonic activity in the Marmara Sea region, NW Anatolia, *J. Geophys. Res.*, *102*, 27,587–27,601.

Taymaz, T., J. A. Jackson, and D. P. McKenzie (1991), Active tectonics of the north and central Aegean Sea, *Geophys. J. Int.*, *106*, 433–490.

Toksoz, M. N., A. F. Shakal, and A. J. Michael (1979), Space-time migration of earthquakes along the North Anatolian fault zone and seismic gaps, *Pure Appl. Geophys.*, *117*, 1258–1270.

Van der Woerd, J., P. Tapponnier, X. Xiwei, B. Meyer, F. Ryerson, and A. S. Mériaux (2001), Rapid active thrusting along the northwestern range front of the Tanghe Nan Shan (Western Gansu, China), *J. Geophys. Res.*, *106*, 30,475–30,504.

Van der Woerd, J., A. S. Mériaux, Y. Klinger, F. J. Ryerson, Y. Gaudemer, and P. Tapponnier (2002a), The 14 November 2001, Mw = 7.8 Kokoxili earthquake in northern Tibet (Qinghai Province, China), *Seismol. Res. Lett.*, *73*(2), 125–135.

Van der Woerd, J., P. Tapponnier, F. Ryerson, A. S. Mériaux, B. Meyer, Y. Gaudemer, R. Finkel, M. Caffee, G. Zhao, and Z. Xu (2002b), Uniform post-glacial slip-rate along the central 600 km of the Kunlun Fault (Tibet), from ^{26}Al, ^{10}Be and ^{14}C dating of riser offsets, and climatic origin of the regional morphology, *Geophys. J. Int.*, *148*, 356–388.

Wallace, R. E. (1981), Active faults, paleoseismology, and earthquake hazards in the western United States, in *Earthquake Prediction: An International Review*, *Maurice Ewing Ser.*, vol. 4, edited by D. W. Simpson and P. G. Richards, pp. 209–216, AGU, Washington, D. C.

Wesnousky, S. G., and C. H. Jones (1994), Oblique slip, slip partitioning, spatial and temporal changes in the regional stress field, and the relative strength of active faults in the Basin and Range, western United States, *Geology*, *22*, 1031–1034.

Westaway, R. (1994), Present-day kinematics of the Middle East and eastern Mediterranean, *J. Geophys. Res.*, *99*(B6), 12,071–12,090.

Wong, H. K., T. Lüdman, A. Ulug, and N. Görür (1995), The Sea of Marmara: A plate boundary sea in an escape tectonic regime, *Tectonophysics*, *244*, 231–250.

Wright, T., E. Fielding, and B. Parsons (2001), Triggered slip: Observations of the 17 August 1999 Izmit (Turkey) earthquake using radar interferometry, *Geophys. Res. Lett.*, *28*, 1079–1082.